

# Vortices in Spatially Inhomogeneous Superfluids

Daniel E. Sheehy and Leo Radzihovsky

*Department of Physics, University of Colorado, Boulder, CO, 80309*

(Dated: June 8, 2004)

We study vortices in a radially inhomogeneous superfluid, as realized by a trapped degenerate Bose gas in a uniaxially symmetric potential. We show that, in contrast to a homogeneous superfluid, an off-axis vortex corresponds to an anisotropic superflow whose profile strongly depends on the distance to the trap axis. One consequence of this superflow anisotropy is vortex precession about the trap axis in the absence of an imposed rotation. In the complementary regime of a finite prescribed rotation, we compute the minimum-energy vortex density, showing that in the rapid-rotation limit it is extremely uniform, despite a strongly inhomogeneous (nearly) Thomas-Fermi condensate density  $\rho_s(r)$ . The weak radially-dependent contribution ( $\propto \nabla^2 \ln \rho_s(r)$ ) to the vortex distribution, that vanishes with the number of vortices  $N_v$  as  $\frac{1}{N_v}$ , arises from the interplay between vortex quantum discreteness (namely their inability to faithfully support the imposed rigid-body rotation) and the inhomogeneous superfluid density. This leads to an enhancement of the vortex density at the center of a typical concave trap, a prediction that is in quantitative agreement with recent experiments. One striking consequence of the inhomogeneous vortex distribution is an azimuthally-directed, radially-shearing superflow.

## I. INTRODUCTION

An essential defining property of a superfluid is the way it responds to an imposed rotation. Because a uniform superfluid state can only support irrotational flow, one might expect a vanishing response to an applied rotation in a simply-connected domain. However, dating back to seminal works of Onsager and Feynman<sup>1,2</sup> it has been understood that a superfluid can indeed rotate, but does so by nucleating localized topological defects (vortices) that carry discrete units of vorticity, thereby revealing the superfluid's macroscopic quantum nature. In a finite system and for a sufficiently low applied rotation rate  $\Omega < \Omega_{c1}$ , the energetic cost of exciting even a single vortex is too high and the superfluid remains stationary. For higher rates, vortices are nucleated into a regular hexagonal lattice that, on average, approximates a uniform response to the applied rigid-body rotation.

In recent years, rapid progress in the field of confined degenerate Bose gases has led to the experimental realization of vortex lattices containing large numbers of vortices<sup>3,4,5,6,7,8,9</sup>. Perhaps the most striking feature of these lattices is their apparent *uniformity* despite the strong spatial variation of the local superfluid density  $\rho_s(r)$  imposed by the trap. Despite some recent attempts<sup>10</sup>, until very recently<sup>11</sup> no simple physical explanation for this uniformity (which has also been observed in simulations<sup>12</sup>) has appeared in the literature.

To emphasize the apparent puzzle that such vortex uniformity presents, one need not look further than the vortex state of a type-II superconductor. There, vortices are well-known to be strongly pinned by (i.e. attracted to) regions of suppressed superfluid density created by material imperfections<sup>13</sup>. Based on this analogy, one might expect that vortices in a confined Bose gas would be repelled from the center of the trap (where superfluid density and therefore vortex kinetic-energy cost is largest), and would congregate near the condensate edges, result-

ing in a highly nonuniform and concave vortex distribution.

In this Paper we present a theory of vortices in a confined spatially-inhomogeneous rotating superfluid, providing a simple physical explanation for and computing corrections to a uniform vortex array. We explicitly calculate the vortex spatial distribution  $\bar{n}_v(r)$  in a trapped degenerate Bose gas characterized by  $\rho_s(r)$ , showing that it is given by

$$\bar{n}_v(r) \simeq \frac{m\Omega}{\pi\hbar} + \bar{c} \nabla^2 \ln \rho_s(r), \quad (1)$$

with  $\bar{c} \equiv (8\pi)^{-1} \ln(e^{-1}/\xi^2\omega)$ ,  $m$  the boson mass,  $\xi$  the vortex core size and  $\omega \equiv m\Omega/\hbar$  the scaled rotation velocity. Since typically the spatial variation of the Thomas-Fermi (TF) condensate density (or  $\rho_s(r)$ , see Ref. 14) takes place on the scale of the condensate radius  $R(\Omega)$ , the  $r$ -dependent correction in  $\bar{n}_v(r)$  (second term) to the uniform rigid-body result  $n_{v0} \equiv m\Omega/\pi\hbar$  is subdominant in the thermodynamic and large rotation limits, vanishing as  $1/N_v$  with increasing number of vortices. More explicitly, for an isotropic harmonic trap, in the Thomas-Fermi approximation we find

$$\bar{n}_v(r) \simeq n_{v0} - \frac{1}{2\pi} \frac{R^2}{(R^2 - r^2)^2} \ln \frac{e^{-1}}{\xi^2\omega}, \quad (2)$$

where the condensate radius  $R(\Omega) = R_0/\sqrt{1 - (\Omega/\Omega_t)^2}$  is swelled by the centrifugal force beyond the Thomas-Fermi trap radius  $R_0$ , diverging as the rotational velocity approaches the trap frequency  $\Omega_t$ .

Hence we show that, indeed, consistent with experiments<sup>4,5,6,7,8,9</sup>, the vortex density is highly uniform and is well-approximated by the rigid-body result. This uniformity can be most transparently understood by ignoring vortex discreteness (valid at high rotation rates<sup>15,16</sup>) and thinking in terms of the energetically optimum superfluid velocity  $\mathbf{v}_s(\mathbf{r})$ . In a nut-

shell, for an arbitrary smoothly-varying superfluid density  $\rho_s(r)$ , the superfluid velocity of the rigid-body form  $\mathbf{v}_s^0 \equiv \Omega \hat{\mathbf{z}} \times \mathbf{r}$ , which corresponds to the uniform vortex density  $n_{v0} = \frac{m}{h} \nabla \times \mathbf{v}_s^0$ , always minimizes the boson's London free-energy. In terms of vortices, this nearly uniform vortex distribution  $\bar{n}_v \approx n_{v0}$  is a consequence of a balance between the spatial variation of the kinetic energy per vortex and the vortex chemical potential, both of which scale with  $\rho_s(r)$ . While it is energetically costlier to position vortices in a region where  $\rho_s(r)$  is high (i.e. the center of the trap), the vortex chemical potential (controlled by  $\rho_s(r)\Omega$ ) is also high there, compensating and leading to an approximately uniform vortex density. The breakdown of the analogy with vortices in type-II superconductors is therefore due to the difference in the spatial dependence of the vortex chemical potential in the two cases. While in superconductors this role is played by a *uniform* external magnetic field  $H$ , in trapped superfluids the vortex chemical potential is proportional to  $\rho_s(r)$  and thus spatially nonuniform.

As we show here, a spatially-dependent correction to  $\bar{n}_v(r)$  in Eq. (1) arises from vortex discreteness and the related inability of the vortex state to locally reproduce the uniform vorticity  $\mathbf{v}_s^0$  corresponding to rigid-body rotation. As shown rigorously long ago by Tkachenko<sup>17</sup>, in the case of a *uniform* superfluid the resulting energetic frustration cannot be reduced and the energetically optimum vortex distribution is a regular vortex lattice with density  $n_{v0}$ . In contrast, in an *inhomogeneous* condensate the associated kinetic energy-density cost is radially-dependent and can be lowered by a nonuniform vortex distribution. As illustrated in Fig. 1, our analytical prediction for  $\bar{n}_v(r)$ , Eq. (2), is indeed experimentally observable and shows remarkable agreement with recent JILA experiments<sup>9</sup>. Furthermore, as we show below, our prediction for the relation between  $\bar{n}_v(r)$  and  $\rho_s(r)$ , Eq. (1), can be more directly experimentally tested by introducing a known inhomogeneity to  $\rho_s(r)$  (by modifying the trap potential) and studying the induced changes in  $\bar{n}_v(r)$ . Despite the deviation of the vortex density from the rigid-body value, within the London regime, the feedback effect on the condensate density  $\rho_s(r)$  is negligible, which remains well-approximated by the Thomas-Fermi expression<sup>18,19</sup>.

One immediate consequence of our prediction of the deviation of  $\bar{n}_v(r)$  from the rigid-body value  $n_{v0}$  is a finite superfluid flow in the reference frame of the lattice (rotating with frequency  $\Omega$  relative to the lab frame). Even more interestingly, the inhomogeneous vortex distribution  $\bar{n}_v(r)$  implies that the resulting azimuthal superflow in fact exhibits a radial shear, as schematically illustrated in Fig. 2.

A prerequisite to the study of the thermodynamic vortex state under a finite imposed rotation (which was our primary initial goal) is the understanding of the single vortex problem. Although a number of interesting results for the few-vortex problem have appeared in the literature<sup>20,21,22,23,24,25,26</sup>, to our knowledge no explicit,

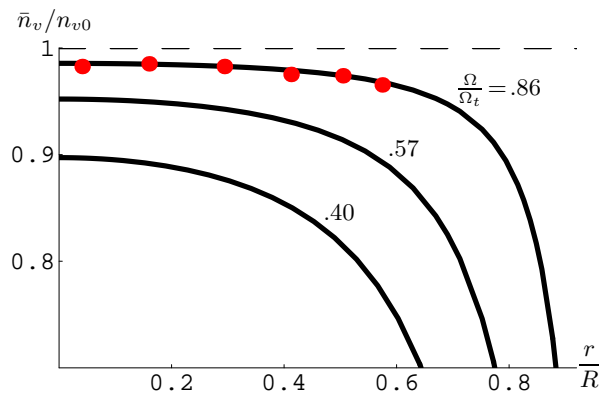


FIG. 1: (Color online) Plot of vortex density for the case of a harmonic trap as a function of radius, Eq. (2) (normalized to  $n_{v0}$ , dashed line), for the following  $\Omega$  and  $R$  values (labelled by the former):  $\Omega = .86\Omega_t$  and  $R = 49\mu m$ ;  $\Omega = .57\Omega_t$  and  $R = 31\mu m$ ;  $\Omega = .40\Omega_t$  and  $R = 25\mu m$ . Points denote data adapted from I. Coddington et al<sup>9</sup>.

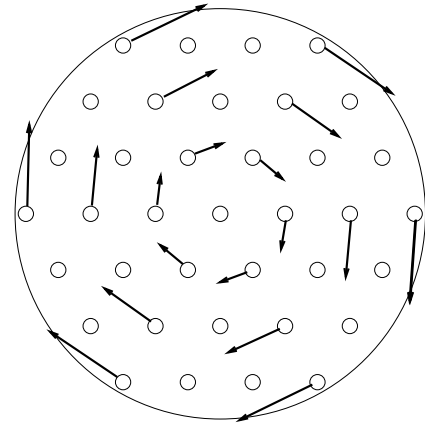


FIG. 2: Schematic plot of the mean superfluid velocity (arrows) along with vortex positions (circles) in the frame rotating counter-clockwise at  $\Omega$  (in which the *lattice is static*). Thus, because  $\mathbf{v}_s \neq \Omega \hat{\mathbf{z}} \times \mathbf{r}$  (and has a magnitude less than it), the superfluid flows past the lattice in the clockwise direction.

full solution for the velocity  $\mathbf{v}_s(\mathbf{r}) = (\hbar/m)\nabla\theta(\mathbf{r})$  around a vortex in an inhomogeneous superfluid has been published. Studying this problem in the London approximation (valid deep in the superfluid state), we find<sup>20,25,27</sup>, that the phase gradient at position  $\mathbf{r}$  near a vortex located off-axis at position  $\mathbf{r}_0$  is given by

$$\nabla\theta(\mathbf{r}) = \frac{\hat{\mathbf{z}} \times (\mathbf{r} - \mathbf{r}_0)}{(\mathbf{r} - \mathbf{r}_0)^2} + \nabla\theta_a(\mathbf{r}), \quad (3a)$$

$$\nabla\theta_a(\mathbf{r}) \simeq \frac{\hat{\mathbf{z}} \times \nabla\rho_s(\mathbf{r}_0)}{2\rho_s(\mathbf{r}_0)} \ln \frac{|\mathbf{r} - \mathbf{r}_0|}{R}, \quad (3b)$$

with  $\nabla\theta_a(\mathbf{r})$  giving the anisotropic correction to the standard uniaxially-symmetric (homogeneous superfluid) result (first term in Eq. (3a)). This additional *curl-free* contribution to the superflow has interesting consequences for the dynamics of individual vortices in an inhomogeneous superfluid. Recall first that, in the absence of external forces, a vortex moves with the local super-

fluid velocity. For the case of a vortex in a spatially inhomogeneous superfluid,  $\nabla\theta_a(\mathbf{r})$  makes an additional contribution to this superflow, leading to the remarkable result (also discussed for specific trap potentials in Refs. 21,22,23,24) that a single vortex at radius  $r$  in an inhomogeneous superfluid will precess about the trap's axis of symmetry with frequency

$$\omega_p \approx \frac{\hbar}{mr} \frac{|\partial_r \rho_s|}{2\rho_s} \ln \frac{R}{\xi}. \quad (4)$$

Such precession has been seen experimentally in Ref. 28 with a quality factor of order 10. We also demonstrate that a pair of vortices near the center of the trap exhibit center-of-charge rotation about the trap while also rotating about each other. The precession rate reassuringly vanishes for uniform  $\rho_s$  in the thermodynamic limit, in which even an off-axis vortex is a stationary state.

In the opposite limit, for  $\mathbf{r}$  far away from the off-axis vortex at  $\mathbf{r}_0$ , the additional contribution to the superflow induced by condensate inhomogeneity has the form of a dipole field due to a opposite-charge vortex at  $\mathbf{r}_0$  and a vortex at the center of the trap. Hence this analytical dipole contribution in the far field effectively shifts the vortex to the center of the trap, leading to a superflow that, far from the vortex, is axially symmetric, circulating around the trap center and described by the phase-gradient  $\nabla\theta = \frac{\mathbf{z} \times \mathbf{r}}{r^2}$ .

The rest of the paper is organized as follows. In Sec. II we use a mean-field model (appropriate for our interests here) for a rotating trapped Bose condensate to recall some standard results and to derive the London equations for the superfluid velocity in the vortex state. In Sec. III we solve these equations to find the superflow around a single off-axis vortex in an inhomogeneous condensate for a number of experimentally-motivated condensate profiles. We then use these results in Sec. IV to derive precessional dynamics in one- and two-vortex problems. In Sec. V we study the many-vortex state and derive our primary result quoted in the Introduction, namely the relation between the vortex and superfluid densities. In Sec. VI, we derive a vortex lattice elastic energy in an inhomogeneous condensate and use it to calculate the Tkachenko mode equations (in the incompressible limit) for a spatially-varying condensate profile. We conclude in Sec. VII with a summary of our results and an outlook to future research.

## II. MODEL OF A TRAPPED (INHOMOGENEOUS) ROTATING SUPERFLUID

The starting point of our analysis is the ground-state energy density of an interacting rotating trapped Bose gas. To eliminate any explicit time dependence, it is convenient to work in the frame of reference in which the boundary conditions and the thermal cloud (the “normal” fluid, playing the role of the proverbial bucket) are stationary<sup>2</sup>. For simplicity, we focus on a trap with a high

degree of uniaxial anisotropy which reduces the problem to two-dimensions perpendicular to the ( $z$ -) axis of rotation, although our work can be straightforwardly generalized to three dimensions. The corresponding boson energy density, written in a reference frame rotating at frequency  $\Omega$ , is given by<sup>29</sup>

$$\varepsilon = \frac{\hbar^2}{2m} |\nabla\Phi|^2 + (V(\mathbf{r}) - \mu)|\Phi|^2 + \frac{g}{2} |\Phi|^4 - \Omega L_z, \quad (5)$$

where the rotation frequency  $\Omega$  plays the role of the “chemical potential” for angular momentum  $L_z$  with

$$\Omega L_z = \Omega \Phi^\dagger [-i\hbar \hat{\mathbf{z}} \cdot (\mathbf{r} \times \nabla)] \Phi. \quad (6)$$

Here,  $V(\mathbf{r})$  is the trapping potential,  $\mu$  is the boson number chemical potential, and  $g$  is the s-wave scattering potential. Expressing the energy density in terms of the condensate density  $\rho_s(\mathbf{r})$ <sup>14</sup> and phase  $\theta(\mathbf{r})$ , defined through the condensate field  $\Phi(\mathbf{r}) = \sqrt{\rho_s} e^{i\theta}$ , (which microscopically is the macroscopically-occupied single-particle wavefunction) we find

$$\varepsilon = \frac{\hbar^2}{2m} [(\nabla\sqrt{\rho_s})^2 + \rho_s(\nabla\theta)^2] + (V(\mathbf{r}) - \mu)\rho_s + \frac{g}{2}\rho_s^2 + i\hbar\Omega(\hat{\mathbf{z}} \times \mathbf{r}) \cdot [\sqrt{\rho_s} \nabla\sqrt{\rho_s} + i\rho_s \nabla\theta]. \quad (7)$$

Deep within a dense Bose-condensed state, where  $\rho_s(\mathbf{r})$  is large, it is convenient to eliminate the superfluid density from Eq. (7) by solving the corresponding Euler-Lagrange equation

$$0 = -\frac{\hbar^2}{2m} [\nabla^2 \sqrt{\rho_s} - \sqrt{\rho_s}(\nabla\theta)^2] + (V(\mathbf{r}) - \mu)\sqrt{\rho_s} + g\rho_s^{3/2} - \hbar\Omega\sqrt{\rho_s}(\hat{\mathbf{z}} \times \mathbf{r}) \cdot \nabla\theta. \quad (8)$$

Neglecting derivatives in  $\rho_s(r)$  and replacing  $\nabla\theta$  by its approximate rigid-body value (see Sec. II A below)  $\nabla\theta \simeq \omega \hat{\mathbf{z}} \times \mathbf{r}$ , we have the usual Thomas-Fermi (TF) result<sup>30</sup>

$$\rho_s(\mathbf{r}) \approx (\mu - V(\mathbf{r}) + \frac{1}{2}m\Omega^2 r^2)/g, \quad (9)$$

for the condensate density profile. For the experimentally most relevant case of a harmonic trap  $V(r) = \frac{1}{2}m\Omega_t^2 r^2$  with  $\Omega_t$  the trap frequency, Eq. (9) is uniaxially isotropic:

$$\rho_s(r) \approx (\mu - \frac{1}{2}m(\Omega_t^2 - \Omega^2)r^2)/g, \quad (10)$$

with the TF cloud radius  $R(\Omega)$  (defined by the radius where  $\rho_s(r)$  vanishes) given by

$$R(\Omega) = \frac{R_0}{\sqrt{1 - (\Omega/\Omega_t)^2}}, \quad (11)$$

and  $R_0 = \sqrt{2\mu/m\Omega_t^2}$  the cloud radius at zero rotation. Using this solution of Eq. (8) inside Eq. (7) and dropping

unimportant constant terms we find the London energy-functional for a rotating superfluid

$$E = \frac{\hbar^2}{2m} \int d^2r \rho_s(\mathbf{r}) [(\nabla\theta)^2 - 2\omega(\hat{\mathbf{z}} \times \mathbf{r}) \cdot \nabla\theta], \quad (12)$$

with  $\omega \equiv m\Omega/\hbar$ .

Under an imposed rotation, a superfluid turns by nucleating vortices. In the London limit these are point singularities at a set of positions  $\mathbf{r}_i$  where the phase  $\theta(\mathbf{r})$  is nonanalytic and satisfies

$$\nabla \times \nabla\theta(\mathbf{r}) = 2\pi n_v(\mathbf{r})\hat{\mathbf{z}}, \quad (13a)$$

$$n_v(\mathbf{r}) = \sum_{i=1} \delta^{(2)}(\mathbf{r} - \mathbf{r}_i), \quad (13b)$$

with  $n_v(\mathbf{r})$  the vortex density. Eqs. (13a),(13b), together with the phase Euler-Lagrange equation ( $\frac{\delta E}{\delta\theta} = 0$ , with  $E$  from Eq. (12))

$$0 = \nabla \cdot (\rho_s(\mathbf{r})\nabla\theta) - \omega\nabla\rho_s(\mathbf{r}) \cdot (\hat{\mathbf{z}} \times \mathbf{r}), \quad (14a)$$

$$= \nabla \cdot (\rho_s(\mathbf{r})\nabla\theta), \quad (14b)$$

determine the superfluid phase  $\theta(\mathbf{r})$  and the corresponding superfluid velocity  $\mathbf{v}_s(\mathbf{r}) = \frac{\hbar}{m}\nabla\theta$ . Here, Eq. (14b) applies for the case of a static trap ( $\omega = 0$ ) or, for a rotating trap in the experimentally relevant case of uniaxial trap symmetry (i.e.  $\rho_s(\mathbf{r}) = \rho_s(r)$ ). It is important to note that the vortex positions  $\mathbf{r}_i(t)$  (and therefore  $n_v(\mathbf{r})$ ) are static in the frame rotating with the vortex lattice; thus, our time-independent expressions containing  $n_v(\mathbf{r})$  are defined in that frame. We shall assume that vortices are static in the frame rotating with the normal component, i.e., at frequency  $\Omega$ .

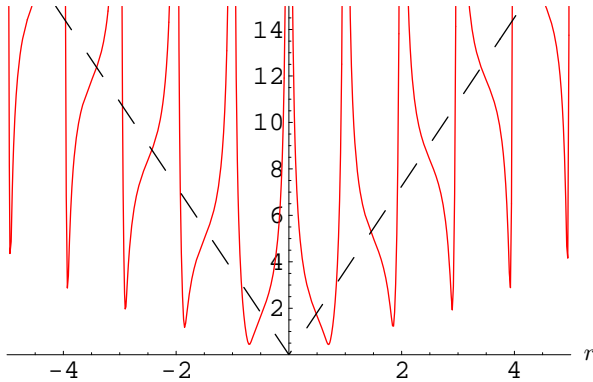


FIG. 3: (Color online) Magnitude of the phase gradient along a line intersecting vortices in a hexagonal rigid-body lattice (solid curve). For comparison, the dashed curve shows the rigid-body result.

### A. Rigid-body result

As noted in the Introduction, the vortex discreteness embodied in Eq. (13b) makes the minimization of  $E$ ,

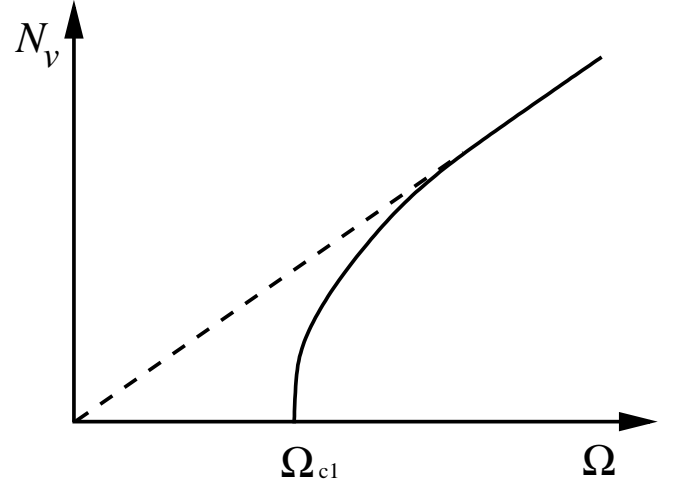


FIG. 4: Schematic depiction of the number of vortices  $N_v$  as a function of the applied rotation rate  $\Omega$  of a finite superfluid. The solid line is the expected actual number of vortices starting at the lower critical angular frequency  $\Omega_{c1}$  whereas the dashed line is the rigid-body result (see main text).

summarized by Eqs. (12),(13a) and (14b), a nontrivial problem. For fast rotation (large  $\Omega$ , such that the coherence length  $\xi$  is comparable to the vortex spacing  $a$ ), the vortex state is dense and we can neglect vortex discreteness, approximating  $\mathbf{v}_s(\mathbf{r})$  and  $n_v(\mathbf{r})$  by arbitrary smooth functions. Expressing  $E$  in Eq. (12) in terms of  $\mathbf{v}_s(\mathbf{r})$  (and dropping a constant), we have

$$E \simeq \frac{m}{2} \int d^2r \rho_s(r) (\mathbf{v}_s - \Omega(\hat{\mathbf{z}} \times \mathbf{r}))^2, \quad (15)$$

which is clearly minimized by the rigid-body solution

$$\mathbf{v}_s = \Omega\hat{\mathbf{z}} \times \mathbf{r}, \quad (16)$$

corresponding to a *uniform* vortex density  $n_{v0} = \omega/\pi = m\Omega/\pi\hbar$ .

Clearly, this rigid-body result for  $\mathbf{v}_s$  cannot be correct for an arbitrary rotation rate  $\Omega$  for the simple reason that it corresponds to a uniform curl of  $\nabla\theta(\mathbf{r})$ , in contrast to Eq. (13a). This discrepancy can also be seen by comparing a numerically computed magnitude of the exact superfluid velocity for a uniform lattice of vortices to that for the rigid-body result, Eq. (16). In Fig. 3 we plot  $|\nabla\theta(\mathbf{r})|$  satisfying Eq. (13a) for a hexagonal array of vortices along a cut through several vortices, and compare it to the rigid-body phase gradient plotted as a dashed line.

### B. Lower critical velocity of a rotating superfluid

Before embarking on a proper calculation of the vortex density,  $n_v(\mathbf{r})$ , that correctly incorporates vortex discreteness, we recall an elementary manifestation of the discrete nature of vortices in the opposite limit of low

$\Omega$ , namely the existence of a lower-critical (imposed) rotation rate  $\Omega_{c1}$  below which the superfluid “refuses” to rotate<sup>31</sup>. To compute  $\Omega_{c1}$ , we simply compare the energy Eq. (12) of a single vortex at the origin to the system’s energy in the absence of vortices. The frequency where they cross is  $\Omega_{c1}$ . For  $\Omega > 0$ , the solution of Eqs. (13a),(14b) for a vortex at the origin leads to a counter-clockwise circulation:

$$\nabla\theta = \frac{\hat{\phi}}{r}. \quad (17)$$

For simplicity, we take for  $\rho_s(\mathbf{r})$  a simple form that is given by a constant  $\rho_0$  inside a radius  $R$  and zero outside this radius. Thus, inserting Eq. (17) into Eq. (12) and evaluating the integral we have

$$E = \frac{\hbar^2 \rho_0}{2m} [2\pi \ln \frac{R}{\xi} - 2\pi\omega R^2], \quad (18)$$

where  $\xi$  is the size of the vortex core derivable from Eq. (8) in the presence of a vortex and providing a short-distance cutoff for London theory. Since clearly for the case of no vortex  $E = 0$ , we find a well-known result for a superfluid confined to radius  $R$  (see, e.g., Ref. 32)

$$\Omega_{c1} = \frac{\hbar}{mR^2} \ln \frac{R}{\xi}, \quad (19)$$

which, unlike the analogous problem of type-II superconductors (because of the absence of screening, i.e., an infinite London penetration length), vanishes in the thermodynamic limit. Since vortices do not appear for  $\Omega < \Omega_{c1}$ , Eq. (19) gives the first hint of the violation of the rigid-body result. This suggests that even for  $\Omega > \Omega_{c1}$  the actual number of vortices  $N_v(\Omega)$  is expected to be *less* than the rigid-body result to which it must asymptotically approach in the large  $\Omega$  limit. Therefore, based on these general arguments we expect  $N_v(\Omega)$  to follow the solid curve in Fig. 4.<sup>33,34</sup>

Thus far, we have provided elementary calculations exhibiting the limiting behavior of a rotating confined Bose gas in the extreme large<sup>15</sup> and small  $\Omega$  regimes. Before turning to the general many-vortex problem, in the next section, we first study the (prerequisite) single vortex problem in a spatially inhomogeneous superfluid.

### III. SINGLE VORTEX IN A SPATIALLY INHOMOGENEOUS SUPERFLUID

In spite of its importance to understanding vortex states in inhomogeneous rotating condensates, the single vortex problem in an trapped rotating BEC has received relatively little attention, with most treatments using the standard homogeneous-condensate vortex solution as a starting point and focusing on dynamics<sup>20,21,22,23,24,25,26</sup>. Two notable exceptions are works by Rubinstein and Pismen<sup>20</sup> and by Svidzinsky and Fetter<sup>25</sup>. However, because of the focus in Ref. 25 on the single-vortex dynamics,

only asymptotics of the superfluid velocity near an off-axis vortex was worked out. On the other hand, although an exact solution for a single vortex was found in Ref. 20, it corresponds to a very special (i.e. not motivated by any experimental realization)  $\rho_s(\mathbf{r})$ .

In contrast, our interest in computing the vortex density distribution (Sec. V) requires a full analysis of the superflow corresponding to a single off-axis vortex in an inhomogeneous condensate and this is the subject of this section. To determine the correct superfluid velocity, we study the Euler-Lagrange equation for  $\theta$  Eq. (14b) (which expresses the conservation of the boson number current) along with the vorticity constraint for a vortex at  $\mathbf{r}_0$ :

$$\nabla \times \nabla\theta = 2\pi\delta^{(2)}(\mathbf{r} - \mathbf{r}_0). \quad (20)$$

For the most general problem, these equations must be supplemented by a boundary condition  $\hat{n} \cdot (\rho_s(\mathbf{r})\nabla\theta)|_R = 0$  enforcing the vanishing of boson current through the boundary of the system. Consequently, the energy and dynamics of a vortex are strongly affected by both the condensate inhomogeneity and the nontrivial boundary conditions<sup>35</sup>. However, for the case of a Bose gas trapped by a smooth potential (relevant to experiments), the condensate density  $\rho_s(\mathbf{r})$  vanishes at the cloud’s boundary, automatically satisfying the above vanishing current condition.

Before analyzing Eqs. (14b) and (20) in detail, we note that (inspired by the vortex solution  $\nabla\theta = \frac{\hat{z} \times (\mathbf{r} - \mathbf{r}_0)}{(\mathbf{r} - \mathbf{r}_0)^2}$  for a uniform superfluid), an exact solution to Eq. (14b) is given by

$$\nabla\theta(\mathbf{r}) = \frac{\rho_s(\mathbf{r}_0)}{\rho_s(\mathbf{r})} \frac{\hat{z} \times (\mathbf{r} - \mathbf{r}_0)}{(\mathbf{r} - \mathbf{r}_0)^2}. \quad (21)$$

Although this solution fails to satisfy Eq. (20) (satisfying it only to leading order in spatial gradients of  $\rho_s(\mathbf{r})$ ) and therefore is not a proper vortex solution, it *does* exhibit the qualitatively correct behavior that we shall verify in this section:  $\nabla\theta$  (and therefore the superfluid velocity) is generally larger where  $\rho_s(\mathbf{r})$  is small and smaller where  $\rho_s(\mathbf{r})$  is large, relative to the solution for a uniform  $\rho_s$ .

For a full and systematic analysis, it is convenient to represent

$$\theta(\mathbf{r}) = \theta_v(\mathbf{r}) + \theta_a(\mathbf{r}), \quad (22)$$

in terms of the known singular part

$$\theta_v(\mathbf{r}) = \tan^{-1} \left[ \frac{y - y_0}{x - x_0} \right], \quad (23a)$$

$$= \phi, \quad (23b)$$

corresponding to a vortex for a uniform superfluid density, with

$$\nabla\theta_v(\mathbf{r}) = \frac{\hat{z} \times (\mathbf{r} - \mathbf{r}_0)}{(\mathbf{r} - \mathbf{r}_0)^2}, \quad (24)$$

that ensures the vortex carries the correct topological charge in Eq. (20). The analytic part  $\theta_a(\mathbf{r})$  ( $\nabla \times$

$\nabla\theta_a(\mathbf{r}) = 0$ ) is chosen so that  $\theta(\mathbf{r})$  satisfies the Euler-Lagrange equation Eq. (14b), which reduces to

$$\nabla\rho_s \cdot \nabla\theta_a + \rho_s \nabla^2\theta_a = -\nabla\rho_s \cdot \nabla\theta_v. \quad (25)$$

(Henceforth in this section we are restricting attention to the uniaxial symmetry case  $\rho_s(\mathbf{r}) = \rho_s(r)$ .) A virtue of this approach is that it reduces the problem to the analytical solution of Eq. (25) subject to a known “source” field  $-\nabla\rho_s \cdot \nabla\theta_v(\mathbf{r})$ , Eq. (24). In the case of a uniform  $\rho_s$ , Eq. (25) is obviously solved by  $\nabla\theta_a(\mathbf{r}) = 0$ , with  $\nabla\theta = \nabla\theta_v(\mathbf{r})$  reducing to the well-known result Eq. (24). In the presence of a nonzero gradient of  $\rho_s(r)$ ,  $\nabla\theta_a(\mathbf{r})$  generally provides a nontrivial (but curl-free) correction to the superfluid velocity in Eq. (24). In addition, since for a smoothly-varying  $\rho_s(r)$  we expect that  $\nabla\theta$  is *approximately* given by the uniform result Eq. (24), this formulation is naturally set up for a systematic expansion in the small parameter  $\nabla \ln \rho_s$ .

Finally we note that for a vortex at the center of the trap ( $\mathbf{r}_0 = 0$ ),  $\nabla\rho_s \propto -\hat{\mathbf{r}}$  leads to a vanishing of the source term  $-\nabla\rho_s \cdot \nabla\theta_v(\mathbf{r}) = 0$ . Consequently for an on-axis vortex  $\nabla\theta_a(\mathbf{r}) = 0$  and the solution reduces to a simple axially-symmetric result  $\nabla\theta = \nabla\theta_v = \frac{\hat{\mathbf{z}} \times \mathbf{r}}{r^2} = \nabla\phi$ .

Thus, below we naturally focus on the nontrivial case of an off-trap-axis ( $\mathbf{r}_0 \neq 0$ ) vortex. Although for a generic  $\rho_s(r)$  no closed form solution to Eq. (25) is available, a systematic asymptotic analysis in all relevant regimes determined by three length scales (the condensate size  $R$ , the vortex position  $\mathbf{r}_0$  and the displacement from the vortex  $\mathbf{r} - \mathbf{r}_0$ ) is possible and is presented in Secs. III A and III B (near a vortex  $|\mathbf{r} - \mathbf{r}_0| \ll r_0 \ll R$ ) and in Sec. III C (away from the vortex  $r_0 \ll |\mathbf{r} - \mathbf{r}_0|$ ).

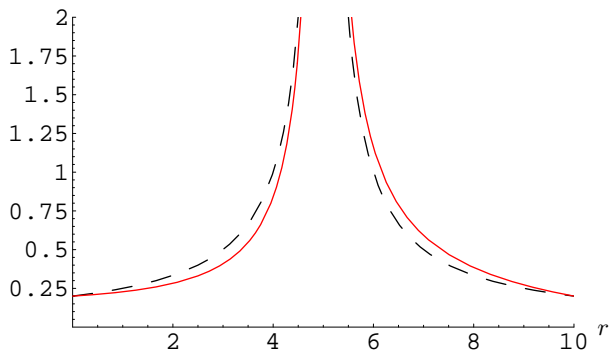


FIG. 5: (Color online) Phase-gradient magnitude (solid curve) through a vortex away from the center of the trap, for the case of the Gaussian condensate profile Eq. (26). The vortex is located at spatial position  $\mathbf{r}_0 = (5, 0)$  with  $R = 5$  characterizing the scale of the condensate. For comparison, the dashed curve depicts  $|\nabla\theta_v|$  only, neglecting the analytic field.

### A. Gaussian condensate profile

Before studying the general case of an arbitrary condensate profile  $\rho_s(r)$ , here we first analyze Eq. (25) for

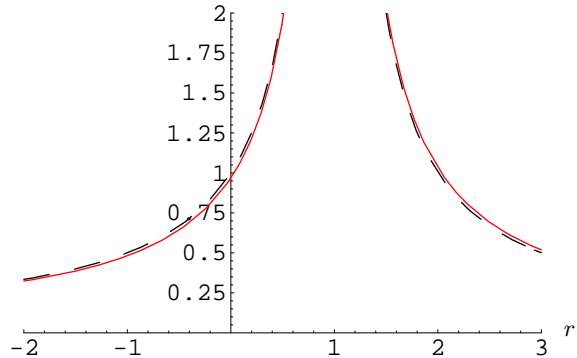


FIG. 6: (Color online) Phase-gradient magnitude (solid curve) through a vortex near the center of the trap, for the case of the Gaussian condensate profile Eq. (26). The vortex is located at spatial position  $\mathbf{r}_0 = (1, 0)$  with  $R = 5$  characterizing the scale of the condensate. For comparison, the dashed curve depicts  $|\nabla\theta_v|$  only, neglecting the analytic field.

the simpler special case of a Gaussian condensate profile

$$\rho_s(r) = \rho_0 \exp(-r^2/2R^2), \quad (26)$$

with  $R$  characterizing the size of the condensate. For this choice, Eq. (25) reduces to

$$-\mathbf{r} \cdot \nabla\theta_a + R^2 \nabla^2\theta_a = \mathbf{r} \cdot \nabla\theta_v. \quad (27)$$

Focusing on the most interesting regime, we solve Eq. (27) in the vicinity of the vortex. Close to the vortex at  $\mathbf{r}_0$ , we can neglect the first term on the left side of Eq. (27) in comparison to the second,  $-\mathbf{r} \cdot \nabla\theta_a + R^2 \nabla^2\theta_a \simeq R^2 \nabla^2\theta_a$ , reducing the equation for  $\theta_a$  to

$$\nabla^2\theta_a = \frac{1}{R^2} \nabla\theta_v \cdot \mathbf{r}. \quad (28)$$

A solution to Eq. (28) is then easily found to be

$$\theta_a(\mathbf{r}) = \frac{1}{2R^2} (\mathbf{r} - \mathbf{r}_0) \cdot (\mathbf{r}_0 \times \hat{\mathbf{z}}) \ln \frac{|\mathbf{r} - \mathbf{r}_0|}{R}, \quad (29)$$

where the denominator of the argument of the logarithm amounts to a choice of integration constant, fixed by matching to an “outer” solution. Our approximate choice above may be motivated physically by noting that we expect  $\theta_a$  to exhibit spatial variation on a scale given by  $R$ , as will be confirmed by more general calculations to follow. Although  $\mathbf{r}_0 \cdot (\mathbf{r}_0 \times \hat{\mathbf{z}}) = 0$ , we have written Eq. (29) in this way to emphasize that close to the vortex, the  $\mathbf{r}$  dependence in  $\theta_a$  arises through the  $\mathbf{r} - \mathbf{r}_0$  combination only.

To emphasize key qualitative features of the solution  $\theta(\mathbf{r})$ , we reexpress the vortex solution in terms of the azimuthal angle  $\phi$  between  $\mathbf{r} - \mathbf{r}_0$  and  $\mathbf{r}_0$ . In terms of  $\phi$  the singular part of the solution is (recall Eq. (23b)) simply  $\theta_v = \phi$ . From Eq. (29) the analytic contribution

$\theta_a(\mathbf{r})$  can be seen to be given by  $\theta_a(\phi) = c \sin \phi$ , leading to

$$\theta(\phi) = \phi + c \sin \phi, \quad (30)$$

with  $c = \frac{1}{2R^2} r_0 |\mathbf{r} - \mathbf{r}_0| \ln \frac{R}{|\mathbf{r} - \mathbf{r}_0|}$ .

An important (required) feature of this solution is that  $\theta_a(\phi)$  is indeed analytic, carrying vanishing winding  $\int_0^{2\pi} d\phi \partial_\phi \theta_a(\phi) = 0$ , and therefore preserving the quantization in units of  $2\pi$  of the winding of the full vortex phase  $\theta(\phi)$ . The consequence of the nontrivial analytic contribution is that  $\theta(\phi)$  obeys this quantization condition by winding more slowly near the center of the trap (i.e. where  $\phi \approx \pi$ ) than away from it (i.e. where  $\phi \approx 0$ ) in agreement with our intuitive approximate vortex solution Eq. (21).

As we illustrate in Fig. 5, the analytical contribution  $\theta_a$  has a small but qualitatively important effect on the superfluid velocity in the vicinity of a vortex. We compare the vortex superfluid velocity magnitude  $|\nabla \theta|$  for a vortex in an inhomogeneous condensate to its counterpart  $|\nabla \theta_v|$  in the homogeneous condensate along  $\hat{\mathbf{x}}$  through the vortex located at  $\mathbf{r}_0 = x_0 \hat{\mathbf{x}}$ . While both velocity profiles exhibit the characteristic  $1/r$  divergence, consistent with our general arguments the superfluid velocity  $|\nabla \theta|$  is clearly smaller than  $|\nabla \theta_v|$  near the center of the trap and larger than it away from the center of the trap, with this effect vanishing (see Fig. 6) for a vortex near the center of the trap.

### B. Generic spatially-varying condensate profile: “inner” solution

We now turn to the full problem of finding the superfluid velocity near a vortex in an inhomogeneous superfluid defined by a general (uniaxially symmetric and smooth, with  $R \gg \xi$ )  $\rho_s(r)$ .

Our method is a simple generalization of the calculation for the Gaussian case in Sec. III A and applies in the regime  $|\mathbf{r} - \mathbf{r}_0| \ll r_0$ . Working to lowest order in the gradient of the condensate profile, near a particular vortex we approximate the smoothly varying  $\rho_s(r)$  and its gradient  $\nabla \rho_s(r)$  by their values at the vortex position  $\mathbf{r}_0$ . This considerably simplifies the Euler-Lagrange equation (while retaining the essential physics) to

$$\nabla \mu(r_0) \cdot \nabla \theta_a(\mathbf{r}) + \frac{1}{2} \nabla^2 \theta_a(\mathbf{r}) = -\nabla \mu(r_0) \cdot \nabla \theta_v, \quad (31)$$

where we defined

$$\nabla \mu(r) \equiv \frac{1}{2} \frac{\nabla \rho_s(r)}{\rho_s(r)}. \quad (32)$$

The solution to Eq. (31) can now be easily obtained by first finding a corresponding Green function that satisfies

$$(\nabla \mu(r_0) \cdot \nabla + \frac{1}{2} \nabla^2) G(\mathbf{r} - \mathbf{r}') = \delta^{(2)}(\mathbf{r} - \mathbf{r}'). \quad (33)$$

An explicit expression for  $G(\mathbf{r})$  (verifiable via direct substitution) may be expressed in terms of the Bessel function  $K_0(x)$ :

$$G(\mathbf{r}) = -\frac{1}{\pi} e^{-\mathbf{r} \cdot \nabla \mu(r_0)} K_0(r |\nabla \mu(r_0)|). \quad (34)$$

This then leads to the solution to Eq. (31) given by

$$\theta_a(\mathbf{r}) = -\int d^2 r' G(\mathbf{r} - \mathbf{r}') \nabla \mu(r_0) \cdot \frac{\hat{\mathbf{z}} \times (\mathbf{r}' - \mathbf{r}_0)}{(\mathbf{r}' - \mathbf{r}_0)^2}, \quad (35a)$$

$$= -\nabla \mu(r_0) \cdot \int d^2 r' G(-\mathbf{r}') \frac{\hat{\mathbf{z}} \times (\mathbf{r}' + \mathbf{r} - \mathbf{r}_0)}{(\mathbf{r}' + \mathbf{r} - \mathbf{r}_0)^2}, \quad (35b)$$

where in going to Eq. (35b) we have shifted the integration variable  $\mathbf{r}' \rightarrow \mathbf{r}' + \mathbf{r}$ , with the resulting integral on the right side clearly a function of  $\mathbf{r} - \mathbf{r}_0$  only (a consequence of our approximation above). Moreover, since the second factor is sharply peaked near  $\mathbf{r}' \simeq \mathbf{r}_0 - \mathbf{r}$ , it is valid to this order of approximation to replace  $G(-\mathbf{r}')$  by its value at this point. The remaining integral may be easily evaluated, finally yielding

$$\begin{aligned} \theta_a(\mathbf{r}) &\approx -(\mathbf{r} - \mathbf{r}_0) \cdot (\hat{\mathbf{z}} \times \nabla \mu(r_0)) e^{-(\mathbf{r} - \mathbf{r}_0) \cdot \nabla \mu(r_0)} \\ &\quad \times K_0(|\mathbf{r} - \mathbf{r}_0| |\nabla \mu(r_0)|), \end{aligned} \quad (36a)$$

$$\approx (\mathbf{r} - \mathbf{r}_0) \cdot (\hat{\mathbf{z}} \times \nabla \mu(r_0)) \ln |\mathbf{r} - \mathbf{r}_0| |\nabla \mu(r_0)|, \quad (36b)$$

where in Eq. (36b) we have taken the  $\mathbf{r} \rightarrow \mathbf{r}_0$  limit of Eq. (36a). Since  $\mu(r)$  varies on the scale of the condensate size  $R$ , the analytical correction  $\theta_a$  scales like  $1/R^2$ , and, as expected, vanishes in the thermodynamic limit.

Using  $\nabla \mu(r_0) = -\hat{\mathbf{r}}_0 |\partial_r \mu(r_0)|$  we find that at fixed distance near the vortex, the azimuthal  $\phi$  dependence of  $\theta(\phi)$  is given by

$$\theta(\phi) \approx \phi + c \sin \phi e^{c' \cos \phi}, \quad (37)$$

with  $c = |\partial_r \mu(r_0)| |\mathbf{r} - \mathbf{r}_0| K_0(|\mathbf{r} - \mathbf{r}_0| |\partial_r \mu(r_0)|)$  and  $c' = |\mathbf{r} - \mathbf{r}_0| |\partial_r \mu(r_0)|$  positive  $\phi$ -independent functions that increase with increasing  $|\mathbf{r} - \mathbf{r}_0|$  (in the stated small  $|\mathbf{r} - \mathbf{r}_0|$  regime). Because of the smallness of  $c'$  near  $\mathbf{r}_0$ , for a Gaussian condensate profile this general result reduces to that found in Sec III A. Again, as required by analyticity of  $\theta_a(\mathbf{r})$ , it is easy to show that  $\int_0^{2\pi} d\phi \partial_\phi \theta_a(\phi) = 0$ , thereby preserving quantization of circulation of superflow encoded in  $\int_0^{2\pi} d\phi \partial_\phi \theta(\phi) = 2\pi$ .

Although the phase (and corresponding superflow) distortion given by  $\theta(\phi)$  is quite small (especially near the vortex) we note that there are a number of experimental techniques that have been used successfully to measure the condensate phase growth around a vortex<sup>3,36</sup>, giving hope that the prediction in Eq. (37) may be experimentally testable.

Using Eq. (36b), the superfluid velocity near a vortex (defined by  $|\mathbf{r} - \mathbf{r}_0| |\nabla \mu(r_0)| \ll 1$ ) is easily computed, giving

$$\begin{aligned} \mathbf{v}_s(\mathbf{r}) &\approx \frac{\hbar}{m} \left[ \frac{\hat{\mathbf{z}} \times (\mathbf{r} - \mathbf{r}_0)}{(\mathbf{r} - \mathbf{r}_0)^2} \right. \\ &\quad \left. + \hat{\mathbf{z}} \times \nabla \mu(r_0) \ln(|\mathbf{r} - \mathbf{r}_0| |\nabla \mu(r_0)|) \right], \end{aligned} \quad (38)$$

in agreement with the result found in Ref. 20. Hence quite generally, near a vortex the correction to the superfluid velocity arising from the inhomogeneity of the condensate is approximately spatially uniform and is orthogonal to the displacement  $\mathbf{r}_0$  from the trap center. We see that, as anticipated based on general arguments above, the superflow is slower at  $\phi = \pi$  and faster at  $\phi = 0$  (see Fig. 7). Moreover, for  $\mathbf{r}_0 \rightarrow 0$ ,  $\nabla\mu(r_0) \rightarrow 0$ , so that the analytic field is negligible for a vortex near the center of the trap.

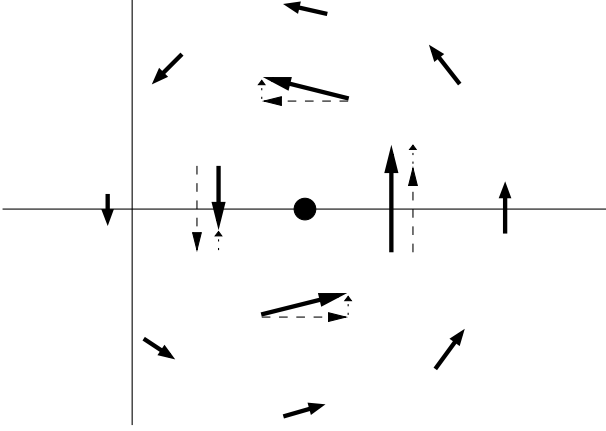


FIG. 7: Schematic picture of the effect of the analytic field on the superfluid velocity of an off-axis vortex (Eq. (38)); the vortex location is denoted by a filled circle. The solid arrows denote  $\nabla\theta$  as affected by the nearly uniform analytic field. On the innermost ring the nearly uniform  $\nabla\theta_a$  is depicted as a small dotted arrow and  $\nabla\theta_v$  is depicted as a larger dashed arrow; their vector sum leads to the distorted  $\nabla\theta$  that is smaller in magnitude near the center of the trap and larger near the edge.

### C. Generic spatially-varying condensate profile: “outer” solution

We now calculate the asymptotics of the superfluid velocity far away from the vortex. Interestingly, after some examination of the form of Eq. (25) it is clear that the outer solution can be easily found. To see this first note that for  $\theta_a$  that satisfies  $\nabla^2\theta_a = 0$  Eq. (24) reduces to

$$\nabla\rho_s \cdot \nabla\theta_a = -\nabla\rho_s \cdot \nabla\theta_v. \quad (39)$$

Naively this would be satisfied by the antivortex (at  $\mathbf{r}_0$ ) solution

$$\nabla\theta_a = -\nabla\theta_v, \quad (40a)$$

$$= -\frac{\hat{\mathbf{z}} \times (\mathbf{r} - \mathbf{r}_0)}{(\mathbf{r} - \mathbf{r}_0)^2}, \quad (40b)$$

(which satisfies the assumed condition  $\nabla^2\theta_a = 0$ ) were it not for the analyticity requirement  $\oint d\mathbf{r} \cdot \nabla\theta_a(\mathbf{r}) = 0$ . However, this is easily fixed by adding to the solution in Eq. (40b) another contribution  $\frac{\hat{\mathbf{z}} \times \mathbf{r}}{r^2}$  due to a positive vortex located at the origin, which clearly satisfies the

homogeneous part of Eq. (25). We thus obtain an *exact* outer solution<sup>37</sup> (verifiable by direct substitution) to Eq. (25):

$$\nabla\theta_a(\mathbf{r}) = \frac{\hat{\mathbf{z}} \times \mathbf{r}}{r^2} - \frac{\hat{\mathbf{z}} \times (\mathbf{r} - \mathbf{r}_0)}{(\mathbf{r} - \mathbf{r}_0)^2}. \quad (41)$$

Because the solution Eq. (41) corresponds to a vortex dipole, with a positive vortex at the trap center and a negative vortex at the location of the true vortex  $\mathbf{r}_0$  it is easy to see that, as required, it satisfies the vanishing circulation ( $\nabla \times \nabla\theta_a = 0$ ) condition for  $|\mathbf{r} - \mathbf{r}_0| \gg r_0$ . Hence far from an off-axis vortex at  $\mathbf{r}_0$ , the superfluid velocity is given by

$$\mathbf{v}_s(\mathbf{r}) \simeq \frac{\hbar}{m} \frac{\hat{\mathbf{z}} \times \mathbf{r}}{r^2}, \quad (42)$$

i.e., the superflow adjusts to be axially symmetric about the trap center, such that a vortex at  $\mathbf{r} = \mathbf{r}_0$  appears to be sitting at  $\mathbf{r} = 0$ .

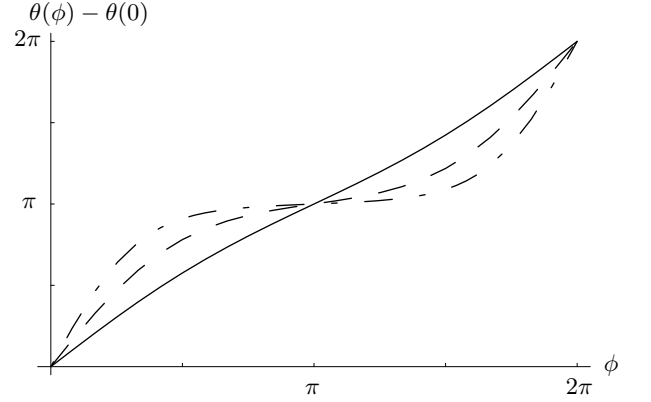


FIG. 8: Plot of the phase around a vortex in an inhomogeneous superfluid for the Bessel profile Eq. (43) as a function of the angle  $\phi$  between  $\mathbf{r} - \mathbf{r}_0$  and  $\mathbf{r}_0$ , for Eq. (44) integrated numerically. The parameters  $R = 10$  and  $r_0 = 20$  and the curves represent  $|\mathbf{r} - \mathbf{r}_0| = 1$  (solid), 10 (dashed) and 100 (dot-dashed).

### D. Bessel condensate profile: Exact solution due to Rubinstein and Pismen

Although we have been unable to find a closed form vortex solution for an arbitrary condensate profile  $\rho_s(r)$ , for a specially contrived but qualitatively realistic profile

$$\rho_s(r) = \frac{\rho_0}{I_0(r/R)^2}, \quad (43)$$

a closed form solution was found by Rubinstein and Pismen in the context of optical vortices in an inhomogeneous laser beam<sup>20</sup>. In Eq. (43),  $I_0(x)$  is the modified



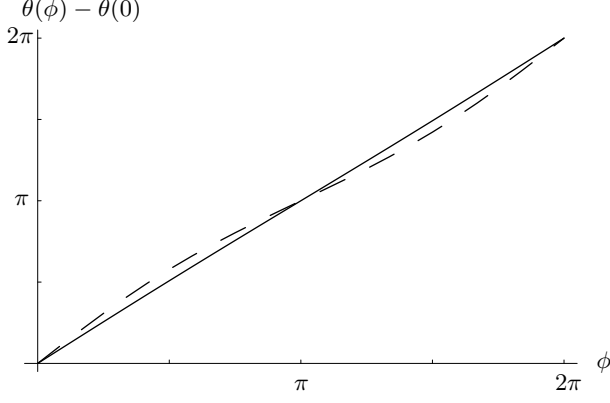


FIG. 9: Same as Fig. 8 but with  $R = 20$ ,  $r_0 = 5$  and  $|\mathbf{r} - \mathbf{r}_0| = 1$  (solid line) and  $|\mathbf{r} - \mathbf{r}_0| = 1000$  (dashed line) exhibiting the smallness of the analytic field for vortices close to the center of the trap.

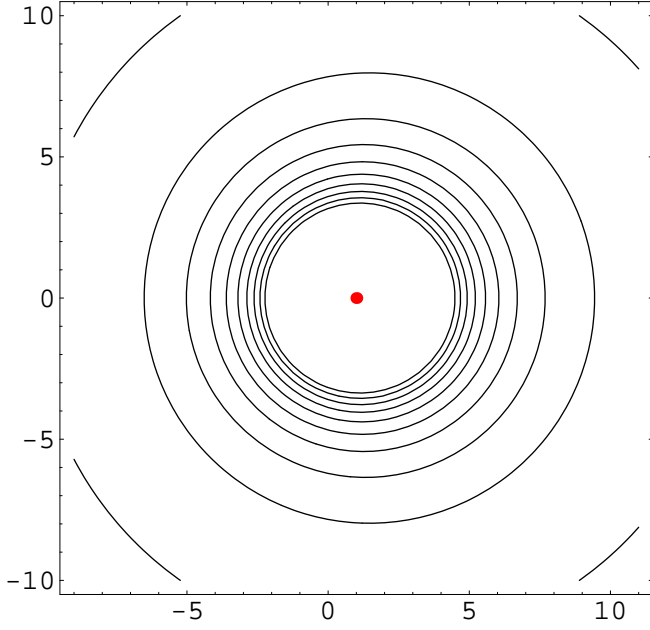


FIG. 10: (Color online) Contour plot of constant phase gradient curves for a vortex at  $\mathbf{r}_0 = (1, 0)$  with  $R = 10$ . Their near-circular symmetry indicates the unimportance of the analytic field in this regime.

Bessel function, with the asymptotic behavior  $I_0(x) \rightarrow 1 + x^2/4$  and  $\exp(x)/\sqrt{2\pi x}$  for  $x \rightarrow 0$  and  $x \rightarrow \infty$ , respectively. This asymptotics shows that this special  $\rho_s(r)$  behaves as  $1 - r^2/2R^2$  for  $r \ll R$  (i.e. it is parabolic) and decays exponentially for  $r \gg R$ . Thus, despite its fine-tuned very specific form, it is qualitatively similar to the experimentally relevant TF profile.

Although most of the properties of a vortex are contained in the asymptotic solutions found in previous sections, it is useful to check the predictions found there for

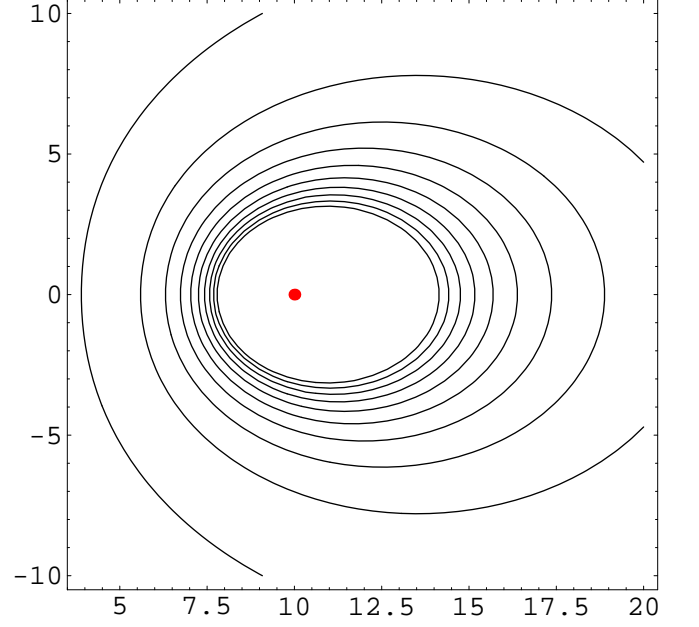


FIG. 11: (Color online) Contour plot of constant phase gradient curves for a vortex at  $\mathbf{r}_0 = (10, 0)$  with  $R = 10$ . The effect of the analytic field is clearly seen in the distorted shapes of these curves; the phase gradient has been decreased to the left of the vortex and increased to the right.

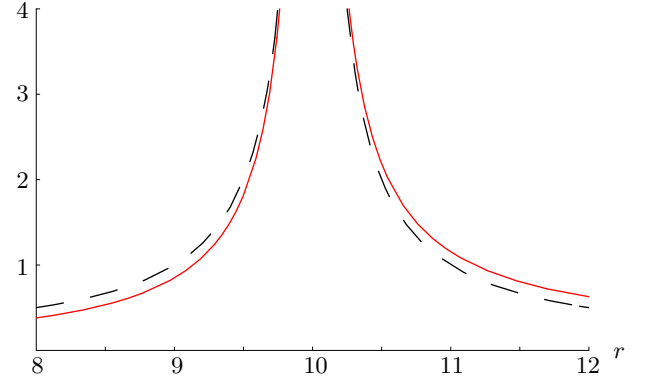


FIG. 12: (Color online) Phase-gradient magnitude (Eq. (44)) through a vortex far from the center of the trap, located at spatial position  $\mathbf{r}_0 = (10, 0)$  with  $R = 10$ . For comparison, the dashed curve depicts  $|\nabla\theta_v|$  only, neglecting the analytic field (solid curve).

a general  $\rho_s(r)$  against the specific but exact solution for  $\rho_s(r)$  in Eq. (43). This is the subject of present subsection.

Following Ref. 20, the Euler-Lagrange equation (14b) can be solved exactly by introducing an auxiliary function  $\chi$  related to  $\theta$  by  $\rho_s(r)\nabla\theta = \hat{\mathbf{z}} \times \nabla\chi$ . With this transformation and the very special choice of  $\rho_s(r)$  in Eq. (43) the vortex quantization condition Eq. (20) reduces to a simple Helmholtz-like partial differential equation for

$\rho_s^{-1/2}\chi(r)$ , which in turn leads to the solution<sup>20</sup>

$$\nabla\theta(\mathbf{r}) = -e^{\mu(r_0)-\mu(r)}\hat{\mathbf{z}} \times [K_0(|\mathbf{r}-\mathbf{r}_0|/R)\nabla\mu(r) + \nabla K_0(|\mathbf{r}-\mathbf{r}_0|/R)], \quad (44)$$

where  $\mu(r) = -\ln I_0(r/R)$  and  $K_0(x)$  is the Bessel function. In the regime  $r, r_0 \ll R$  of primary interest to us we find (using  $K_0(x) \approx -\ln x$ , for  $x \rightarrow 0$ )

$$\nabla\theta(\mathbf{r}) \simeq \frac{\hat{\mathbf{z}} \times \hat{\mathbf{r}}}{R} \frac{I_1(r/R)}{I_0(r_0/R)} \ln \frac{R}{|\mathbf{r}-\mathbf{r}_0|} + \frac{\hat{\mathbf{z}} \times (\mathbf{r}-\mathbf{r}_0)}{(\mathbf{r}-\mathbf{r}_0)^2} \frac{I_0(r/R)}{I_0(r_0/R)}. \quad (45)$$

For  $\mathbf{r} \rightarrow \mathbf{r}_0$ , the second term dominates inside  $\nabla\theta$ , leaving the first term as a small correction. In this regime, the first curl-free term is the  $\nabla\theta_a$  analytic contribution introduced in Eq. (22). Thus, this exact result agrees with the general one found in Eq. (38) and discussed in the Introduction, Eq. (3a).

In the opposite regime, far away from the vortex ( $r \gg r_0$ ), but still away from the condensate boundary ( $r \ll R$ ), the first term continues to be subdominant to the “bare” vortex contribution (second term). However, its  $\mathbf{r}$  dependence can no longer be ignored and leads to a superflow that is perpendicular to the position vector  $\mathbf{r}$ , rather than the vortex position vector  $\mathbf{r}_0$ .

Even further in the far field, defined by  $r \gg R$  but  $r_0 \ll R$  (so that the vortex is still near the center of the trap)<sup>38</sup>, the exact solution Eq. (44) reduces simply to

$$\nabla\theta(\mathbf{r}) \approx \frac{\hat{\mathbf{z}} \times \mathbf{r}}{r^2}, \quad (46)$$

with small power-law corrections in  $R/r$ , in agreement with our “outer” solution Eq. (41).

The vortex distortion due to the condensate inhomogeneity can also be seen in the angular coordinate dependence of  $\theta(\phi) - \theta(0)$  (obtained by numerically integrating Eq. (44) along a contour between 0 and  $\phi$ ) that we plot in Figs. 8 and 9 for different radii  $|\mathbf{r}-\mathbf{r}_0|$ . As we found in Sec. III A, the distinction between the exact vortex  $\theta(\phi)$  and  $\theta_v(\phi) = \phi$  is largest for vortices far from the center of the trap (see Fig. 8), and grows with  $|\mathbf{r}-\mathbf{r}_0|$ . For a vortex near the center of the trap (Fig. 9), the distinction is barely noticeable. From examining these plots it is clear that an off-axis vortex exhibits an azimuthal dependence of the phase that (as found in Sec. III B) is given by  $\theta(\phi) \approx \phi + c \sin \phi$  with  $c$  a positive constant that grows with distance away from the vortex,  $|\mathbf{r}-\mathbf{r}_0|$ , and with distance of the vortex from the trap axis,  $r_0$ .

To further depict the increasing importance of the analytic field for vortices located away from the center of the trap, in Figs. 10 and 11 we plot (for  $R = 10$ ) contours of constant  $|\nabla\theta|$  for a vortex at  $\mathbf{r}_0 = (1, 0)$  and  $\mathbf{r}_0 = (10, 0)$ , respectively. As expected from earlier discussion, Eq. (38), the superflow of a vortex near the center of the trap (Fig. 10) characterized by nearly circular contours contrasts strongly with that of a far-off-axis

vortex (Fig. 11) described by highly distorted contours of constant superfluid velocity. This latter distortion is a manifestation of our earlier finding of a larger correction to the superfluid velocity for vortices away from the center of the trap and smaller near it. In Fig. 12 we depict the phase-gradient magnitude (solid curve) for the same parameters as Fig. 11, contrasting it with that of a vortex in a homogeneous condensate (dashed curve) given by  $|\nabla\theta_v|$ .

#### IV. PRECESSIONAL DYNAMICS OF INDIVIDUAL VORTICES IN SPATIALLY INHOMOGENEOUS SUPERFLUIDS

Having found in Sec. III the vortex superflow profile in a spatially inhomogeneous superfluid, here we study implications of these results for few-vortex dynamics. In the absence of rotation ( $\Omega = 0 < \Omega_{c1}$ ), vortex excitations are *metastable*, and therefore should eventually escape the condensate, allowing the superfluid to relax to the ground state. However, because of the (massless) guiding-center dynamics of the vortex, which conserves angular momentum, we expect the vortex lifetime to be quite long (limited by the trap’s azimuthal asymmetry and decoherence). As we show in the next subsection, on shorter timescales a vortex in a confined Bose gas, located away from the trap axis, *necessarily* precesses around the center of the trap<sup>22,23,24</sup>. This can be understood from general considerations by noting that energy eigenstates in an axially-symmetric (finite) trap are also angular momentum eigenstates. Consequently, an off-axis point vortex (that clearly is not an eigenstate of angular momentum) is not an energy eigenstate and must therefore evolve at constant energy. As we demonstrate in Appendix A such vortex precession is a property of any confined superfluid, even with a uniform condensate density.

##### A. Precession of a single vortex

We shall now demonstrate (via two different routes) that an off-axis vortex in a spatially inhomogeneous superfluid precesses around the trap center<sup>22,23,24</sup>. To begin, we recall that the dynamics of a vortex is governed by the Magnus “force”<sup>39,40</sup>

$$\mathbf{F}_M = 2\pi\hbar\rho_s\hat{\mathbf{z}} \times (\dot{\mathbf{r}}_i - \mathbf{v}_s), \quad (47)$$

where  $\dot{\mathbf{r}}_i$  is the velocity of the  $i$ th vortex and  $\mathbf{v}_s$  is the background superfluid velocity (not including the symmetric divergent part  $\nabla\theta_v$  due to the vortex itself) at the location of the vortex,  $\mathbf{r}_i$ . In the absence of other forces and in equilibrium  $\mathbf{F}_M = 0$ , giving that a vortex moves at the local superfluid velocity,  $\dot{\mathbf{r}}_i = \mathbf{v}_s$ . In an inhomogeneous superfluid, it is appropriate to identify  $\mathbf{v}_s$  with the curl-free contribution  $\hbar\nabla\theta_a/m$  that, as discussed in Sec. III, arises from condensate inhomogeneity.

Thus, using the second (analytic) term of Eq. (38) with  $|\mathbf{r} - \mathbf{r}_i| \approx \xi$ , we find

$$\dot{\mathbf{r}}_i \simeq \frac{\hbar}{m} \hat{\mathbf{z}} \times \nabla \mu(r_i) \ln \xi |\nabla \mu(r_i)|, \quad (48)$$

where we remind the reader that  $\nabla \mu(r)$  is given by Eq. (32).

The result in Eq. (48) may be also obtained by computing the energy  $E(\mathbf{r}_i)$  of a vortex (corresponding to the kinetic energy of the superfluid) at position  $\mathbf{r}_i$  in an inhomogeneous superfluid. Balancing the associated force against the Magnus “force”<sup>24</sup> gives the equation of motion of the vortex:

$$2\pi\hbar\rho_s\hat{\mathbf{z}} \times \dot{\mathbf{r}}_i - \nabla E(\mathbf{r}_i) = 0, \quad (49)$$

where the curl-free part of the vortex flow  $\nabla\theta_a$  is now regarded as part of the vortex and therefore the external superflow  $\mathbf{v}_s$  in Eq. (49) is taken to be zero. Starting with the kinetic energy, Eq. (12) (at  $\omega = 0$ ), expressing it in terms of  $\theta_v$  and  $\theta_a$ , and using the equation of motion for  $\theta_a$ , Eq. (25), we find

$$E(\mathbf{r}_i) = \frac{\hbar^2}{2m} \int d^2r [\rho_s(r)(\nabla\theta_v)^2 - \rho_s(r)(\nabla\theta_a)^2], \quad (50)$$

with  $\theta_a$  the solution to Eq. (25) and  $\nabla\theta_v$  given by Eq. (24). Because the curl-free superfluid velocity correction  $\frac{\hbar}{m}\nabla\theta_a$  arises from the condensate inhomogeneity, its contribution to the vortex kinetic energy is subdominant, vanishing as  $1/R^2$ . In the dominant (first) term the superfluid velocity  $\frac{\hbar}{m}\nabla\theta_v$  diverges at  $\mathbf{r}_i$ , allowing us to ignore the  $\mathbf{r}$  dependence of the smoothly varying density  $\rho_s(r)$  and approximate it by its value at the vortex,  $\rho_s(r) \simeq \rho_s(r_i)$ . This leads to

$$E(\mathbf{r}_i) \approx \frac{\hbar^2}{2m} \rho_s(r_i) 2\pi \ln \frac{R}{\xi}, \quad (51)$$

which is correct to leading order in the small parameter  $\xi/R$ . When inserted into Eq. (49), we have

$$\dot{\mathbf{r}}_i \simeq -\frac{\hbar}{m} \hat{\mathbf{z}} \times \nabla \mu(r_i) \ln \frac{R}{\xi}, \quad (52)$$

in agreement (up to weak logarithmic corrections) with Eq. (48) found above.

For an axially symmetric trap, with  $\nabla\mu = \hat{\mathbf{r}}\partial_r\mu(r)$ , the equation of motion Eq. (52) can be easily solved and (as advertised) gives vortex precession about the center of the trap:

$$\mathbf{r}_i(t) = r_i(\hat{\mathbf{x}} \cos \omega_p t + \hat{\mathbf{y}} \sin \omega_p t), \quad (53)$$

with the direction of rotation in the same sense as vortex circulation (i.e., counterclockwise here) and with the angular frequency  $\omega_p$  given by:

$$\omega_p = \frac{\hbar}{mr_i} \partial_r \mu(r_i) \ln \frac{\xi}{R}, \quad (54a)$$

$$= \frac{\hbar}{mr_i} \frac{\partial_r \rho_s(r_i)}{2\rho_s(r_i)} \ln \frac{\xi}{R}. \quad (54b)$$

For simplicity, in Eq. (53) we have chosen a particular initial condition  $\mathbf{r}_i(0) = \hat{\mathbf{x}}r_i$ . For the experimentally relevant case of a TF condensate profile  $\rho_s(r) = \rho_0(1 - r^2/R^2)$ , the precession frequency Eq. (54b) reduces to

$$\omega_p = \frac{\hbar}{m} \frac{1}{R^2 - r_i^2} \ln \frac{R}{\xi}, \quad (55)$$

which agrees qualitatively with JILA experiments that observe such precession at angular frequency  $\approx \hbar/mR^2$  that is roughly independent of  $r_i$ <sup>28</sup>.

## B. Precession of multiple vortices

The above analysis can be easily extended to the dynamics of many vortices, where each vortex moves with the local superfluid velocity that is due to the sum of its own curl-free superflow  $\frac{\hbar}{m}\nabla\theta_a$  (generated by the condensate inhomogeneity) and the superflow of all other vortices. For the simplest case of two vortices the equations of motion are given by

$$\dot{\mathbf{r}}_1 = \frac{\hbar}{m} \nabla\theta_{a,1}(\mathbf{r}_1) + \frac{\hbar}{m} \nabla\theta_2(\mathbf{r}_1; \mathbf{r}_2), \quad (56a)$$

$$\dot{\mathbf{r}}_2 = \frac{\hbar}{m} \nabla\theta_{a,2}(\mathbf{r}_2) + \frac{\hbar}{m} \nabla\theta_1(\mathbf{r}_2; \mathbf{r}_1), \quad (56b)$$

where  $\nabla\theta_{a,i}(\mathbf{r}_i)$  is the analytic phase gradient induced by vortex  $i$  at position  $\mathbf{r}_i$  and  $\nabla\theta_i(\mathbf{r}_j; \mathbf{r}_i)$  is the *total* phase gradient induced at position  $\mathbf{r}_j$  due to vortex  $i$  which is located at position  $\mathbf{r}_i$ . Equations (56a) and (56b) are quite general. We now restrict attention to the case of a TF condensate profile and focus on the limit  $r_i \ll R$  so that the rotation frequency Eq. (55) is approximately independent of radius. As we showed in Sec. III,  $\nabla\theta_a$  is almost always much smaller than  $\nabla\theta_v$  (especially when  $r_i \ll R$ ) so that the second terms in Eq. (56a) and Eq. (56b) can be well-approximated by neglecting the associated analytic fields. Under these conditions we have

$$\dot{\mathbf{r}}_1 = \frac{\hbar}{m} \left( \frac{1}{R^2} \hat{\mathbf{z}} \times \mathbf{r}_1 \ln \frac{R}{\xi} + \frac{\hat{\mathbf{z}} \times (\mathbf{r}_1 - \mathbf{r}_2)}{(\mathbf{r}_1 - \mathbf{r}_2)^2} \right), \quad (57a)$$

$$\dot{\mathbf{r}}_2 = \frac{\hbar}{m} \left( \frac{1}{R^2} \hat{\mathbf{z}} \times \mathbf{r}_2 \ln \frac{R}{\xi} + \frac{\hat{\mathbf{z}} \times (\mathbf{r}_2 - \mathbf{r}_1)}{(\mathbf{r}_2 - \mathbf{r}_1)^2} \right). \quad (57b)$$

The two equations decouple when we change variables to relative ( $\boldsymbol{\rho} \equiv \mathbf{r}_1 - \mathbf{r}_2$ ) and center-of-charge ( $\mathbf{R}_c \equiv (\mathbf{r}_1 + \mathbf{r}_2)/2$ ) coordinates:

$$\dot{\boldsymbol{\rho}} = \frac{\hbar}{m} \left( \frac{\ln R/\xi}{R^2} \hat{\mathbf{z}} \times \boldsymbol{\rho} + 2 \frac{\hat{\mathbf{z}} \times \boldsymbol{\rho}}{\rho^2} \right), \quad (58a)$$

$$\dot{\mathbf{R}}_c = \frac{\hbar}{mR^2} \ln \frac{R}{\xi} \hat{\mathbf{z}} \times \mathbf{R}_c, \quad (58b)$$

so that the vortex pair center-of-charge rotates around the origin at the lower-critical frequency  $\Omega_{c1}$

$$\omega_c = \frac{\hbar}{mR^2} \ln \frac{R}{\xi}, \quad (59)$$

and the two vortices orbit each other at frequency

$$\omega_\rho = \frac{\hbar}{m} \left( \frac{1}{R^2} \ln \frac{R}{\xi} + \frac{2}{\rho^2} \right), \quad (60)$$

which increases rapidly with decreasing vortex separation  $\rho$ , with the divergence at  $\rho \rightarrow 0$  (as usual) cut off by the coherence length  $\xi$ .

## V. VORTEX ARRAY IN A SPATIALLY INHOMOGENEOUS SUPERFLUID

We now turn to the many-vortex problem, with the goal of computing the vortex spatial distribution in an inhomogeneous rotating superfluid. The superfluid velocity  $\mathbf{v}_s = \frac{\hbar}{m} \nabla \theta$ , measured in the laboratory frame, due to an array of  $N$  vortices is a solution of Eqs (13a) and (13b) from Sec. II. By linearity of these equations it is given as the sum of the contributions from each vortex:

$$\nabla \theta(\mathbf{r}) = \sum_{i=1}^N \frac{\hat{\mathbf{z}} \times (\mathbf{r} - \mathbf{r}_i)}{(\mathbf{r} - \mathbf{r}_i)^2}, \quad (61)$$

with vortex positions  $\mathbf{r}_i$  static in the frame of the normal component (rotating with frequency  $\Omega$  relative to the lab frame). In the above, we have justifiably neglected the curl-free  $\nabla \theta_a$  contribution to the superflow of a vortex, studied in Sec. III, that, as can be seen from Eq. (38), scales as  $\nabla \rho_s / \rho_s \sim 1/R$  and therefore gives a contribution that is subdominant (in our expansion in  $\nabla \rho_s / \rho_s$ ) in the large condensate limit. Moreover, since  $\nabla \theta_a$  is curl-free it cannot contribute to the rotation of the superfluid and thus is expected to be irrelevant for the rapid-rotation limit. The corresponding vortex density is given by Eq. (13b)

$$n_v(\mathbf{r}) = (2\pi)^{-1} \nabla \times \nabla \theta = \sum_i^N \delta^2(\mathbf{r} - \mathbf{r}_i). \quad (62)$$

As discussed in Sec. II A, for high rotation rates  $\Omega$  the vortex state is dense, and to a high accuracy we can neglect the discrete nature of vortices [embodied by Eqs. (61),(62)] and approximate the superfluid velocity  $\mathbf{v}_s(\mathbf{r})$  and vortex density  $n_v(\mathbf{r})$  by arbitrary smooth functions that minimize the total energy, Eq. (12). As we showed in Sec. II A, within this continuum approximation, the superfluid velocity is simply given by the rigid-body result  $\mathbf{v}_s = \Omega \hat{\mathbf{z}} \times \mathbf{r}$  and  $n_{v0} = m\Omega/\pi\hbar$ , thereby providing a simple explanation for the high vortex lattice uniformity observed in experiments<sup>4,5,6,7,8,9</sup>. Despite this agreement, it is of interest to understand the degree of accuracy and limitations of this uniform vortex distribution (rigid-body) prediction.

Away from this classical rapid-rotation limit<sup>15</sup>, vortex discreteness begins to matter and the rigid-body uniform vortex distribution solution clearly breaks down, as  $\mathbf{v}_s(\mathbf{r})$

diverges as  $1/|\mathbf{r} - \mathbf{r}_j|$  near each vortex at  $\mathbf{r}_j$ . As illustrated in Fig. 3,  $\mathbf{v}_s(\mathbf{r})$  thus strongly deviates from rigid-body flow. In this regime, where a superfluid exhibits its locally irrotational quantum nature, the summation in Eq. (61) can no longer be replaced by an integration, and the minimization of  $E$  must be done directly over vortex positions,  $\mathbf{r}_i$ , rather than over a field  $\mathbf{v}_s(\mathbf{r})$ . In fact, as we saw in Sec. II B, this vortex discreteness manifests itself even in a uniform but finite-size condensate through the lower-critical rotational velocity  $\Omega_{c1} \approx (\hbar/mR^2) \ln \frac{R}{\xi}$  below which no rotation is supported by the condensate.

For a *uniform* infinite condensate the problem was solved long ago by Tkachenko<sup>17</sup>, who rigorously demonstrated that the solution is a hexagonal lattice characterized by the vortex density  $n_{v0}$ . Carrying out Tkachenko's exact analysis for a spatially-varying  $\rho_s(r)$  is a formidable task. We shall instead develop an approximate continuum theory that nevertheless incorporates the essential vortex discreteness and which is valid for a smooth condensate profile  $\rho_s(r)$ , with accuracy controlled by  $\nabla \ln \rho_s$ .

### A. Vortex lattice in a generic inhomogeneous superfluid density profile

We have shown that to compute the vortex distribution in an inhomogeneous condensate, it is essential to faithfully incorporate vortex *discreteness* in treating the sum in Eq. (61). For  $\mathbf{r}$  near a vortex located at  $\mathbf{r}_j$ , the superflow is clearly dominated (see Fig. 3) by a diverging contribution from the  $j$ th vortex, with other vortices making a subleading and *smoothly varying* correction to  $\nabla \theta(\mathbf{r})$ . To formalize this, we write  $\mathbf{r} = \mathbf{r}_j + \delta\mathbf{r}$  and split the sum in Eq. (61) into a contribution from the  $j$ th vortex plus a contribution due to all remaining vortices:

$$\nabla \theta(\mathbf{r}_j + \delta\mathbf{r}) = \frac{\hat{\mathbf{z}} \times \delta\mathbf{r}}{\delta r^2} + \hat{\mathbf{z}} \times \sum_{i \neq j} \frac{\mathbf{r}_j + \delta\mathbf{r} - \mathbf{r}_i}{(\mathbf{r}_j + \delta\mathbf{r} - \mathbf{r}_i)^2}. \quad (63)$$

In the smooth correction to the superflow due to all other vortices the sum over vortex positions can be safely approximated by an integral over a continuously distributed vortex density:

$$\frac{\hbar}{m} \nabla \theta(\mathbf{r}_j + \delta\mathbf{r}) \simeq \frac{\hbar}{m} \frac{\hat{\mathbf{z}} \times \delta\mathbf{r}}{\delta r^2} + \bar{\mathbf{v}}_s(\mathbf{r}_j + \delta\mathbf{r}), \quad (64a)$$

$$\bar{\mathbf{v}}_s(\mathbf{r}) \equiv \frac{\hbar}{m} \int d^2 r' \bar{n}_v(\mathbf{r}') \frac{\hat{\mathbf{z}} \times (\mathbf{r} - \mathbf{r}')}{(\mathbf{r} - \mathbf{r}')^2}, \quad (64b)$$

where  $\bar{n}_v(\mathbf{r})$  and  $\bar{\mathbf{v}}_s(\mathbf{r})$  are the vortex density and superfluid velocity at position  $\mathbf{r}$ , coarse-grained on the scale of the lattice spacing. Equation (64b) may be simplified by expressing the vortex coordinate  $\mathbf{r}_i = \mathbf{r}_i^0 + \mathbf{u}(\mathbf{r}_i^0)$  with the  $\mathbf{r}_i^0$  forming a uniform hexagonal lattice at average density  $n_{v0}$  and  $\mathbf{u}(\mathbf{r})$  being a static vortex displacement field. In terms of  $\mathbf{u}(\mathbf{r})$ ,

$$\bar{n}_v(\mathbf{r}) \simeq n_{v0}(1 - \nabla \cdot \mathbf{u}(\mathbf{r})), \quad (65)$$

so that the integral in Eq. (64b) gives

$$\bar{\mathbf{v}}_s(\mathbf{r}) = \Omega[\hat{\mathbf{z}} \times \mathbf{r} - 2\hat{\mathbf{z}} \times \mathbf{u}_L(\mathbf{r})]. \quad (66)$$

Thus, the coarse-grained part of the superflow is only sensitive to the *longitudinal* vortex displacement, related to  $\mathbf{u}$  through

$$\mathbf{u}_L(\mathbf{r}) = \frac{\nabla \nabla}{\nabla^2} \cdot \mathbf{u}, \quad (67a)$$

$$= \int d^2 r' \nabla G(\mathbf{r} - \mathbf{r}') \nabla \cdot \mathbf{u}(\mathbf{r}'), \quad (67b)$$

with  $G(\mathbf{r} - \mathbf{r}')$  the Green function for the Laplacian. Since (as we will see below) for the case of main interest of an axially-symmetric trap the optimum vortex lattice distortion is purely longitudinal, we may take  $\mathbf{u}_L = \mathbf{u}$ . Equation (64a) is a remarkable result that illustrates how vortices, each with a singular  $\hat{\phi}/r$  superfluid velocity, add up to approximate rigid-body flow<sup>41</sup> with the (second)  $u$ -term characterizing deviations from it.

To compute the vortex distribution  $\bar{n}_v(\mathbf{r})$ , we express the energy Eq. (12) in terms of the vortex lattice displacement field  $\mathbf{u}(\mathbf{r})$  and minimize it over  $\mathbf{u}(\mathbf{r})$ . To this end, we express the energy  $E$  of an array of vortices as a sum over contributions due to individual unit cells, with each cell associated with a particular vortex<sup>42,43</sup>:

$$E = \frac{\hbar^2}{2m} \sum_i \int d^2 r \rho_s(\mathbf{r}) [\nabla \theta(\mathbf{r}) - \omega(\hat{\mathbf{z}} \times \mathbf{r})]^2, \quad (68)$$

where the subscript  $i$  on the integral indicates that it is to be performed over a unit cell centered at  $\mathbf{r}_i$ . In obtaining Eq. (68), we have completed the square in Eq. (12) and discarded a constant term. Using Eq. (64a) for the phase gradient within the  $i$ th cell, shifting the integration in each cell via  $\mathbf{r} \rightarrow \mathbf{r} + \mathbf{r}_i$  and using the fact that  $\rho_s(\mathbf{r})$  does not vary appreciably over a cell (i.e.  $\rho_s(\mathbf{r} + \mathbf{r}_i) \simeq \rho_s(\mathbf{r}_i)$  inside a particular cell), we find

$$E \simeq \frac{\hbar^2}{2m} \sum_i \rho_s(\mathbf{r}_i) \int d^2 r \left[ \frac{\hat{\mathbf{z}} \times \mathbf{r}}{r^2} - 2\omega \hat{\mathbf{z}} \times \mathbf{u}_L(\mathbf{r} + \mathbf{r}_i) \right]^2. \quad (69)$$

The dominant contribution to the energy per cell comes from the diverging superfluid velocity at the center of a cell; thus the way in which we treat the cells' boundary is unimportant. Taking each cell to be a circle of radius  $a$ , set by the average vortex density  $\bar{n}_v(\mathbf{r}) = 1/\pi a^2$  and approximating the smoothly-varying field  $\mathbf{u}_L(\mathbf{r})$  by its value at the vortex position  $\mathbf{u}_L(\mathbf{r} + \mathbf{r}_i) \approx \mathbf{u}_L(\mathbf{r}_i)$ , the integrals over the cell areas can be easily done, giving

$$E \simeq \frac{\hbar^2}{2m} \sum_i \rho_s(\mathbf{r}_i) \left[ \pi \ln \frac{1}{\pi \xi^2 \bar{n}_v} + \frac{4\omega^2 u_L(\mathbf{r}_i)^2}{\bar{n}_v(\mathbf{r}_i)} \right], \quad (70)$$

with the short-scale logarithmic divergence of the vortex kinetic energy as usual cut off by the vortex core size  $\xi$ .

The vortex discreteness effects that we have emphasized, arising from the singular nature of the phase gradient near the core of a vortex, are contained within the

first term of the energy functional Eq. (70) and clearly vanish at high vortex density as  $\pi \xi^2 \bar{n}_v \rightarrow 1$ .<sup>15</sup> The remaining sum over vortex cells can be faithfully approximated by an integral

$$\sum_i \dots = \int d^2 r n_v(\mathbf{r}) \dots, \quad (71a)$$

$$\approx \int d^2 r \bar{n}_v(\mathbf{r}) \dots, \quad (71b)$$

which, after using Eq. (65), finally gives the energy functional of a vortex solid in an inhomogeneous rotating condensate:

$$E[\mathbf{u}(\mathbf{r})] \simeq \frac{\hbar^2}{2m} \int d^2 r \rho_s(\mathbf{r}) \left[ 4\omega^2 u_L(\mathbf{r})^2 + \omega(1 - \nabla \cdot \mathbf{u}(\mathbf{r})) \ln \frac{1}{\xi^2 \omega(1 - \nabla \cdot \mathbf{u})} \right]. \quad (72)$$

Armed with  $E[\mathbf{u}]$ , the vortex distribution can be easily computed by minimizing  $E[\mathbf{u}]$  over  $\mathbf{u}(\mathbf{r})$ , namely by solving  $\frac{\delta E}{\delta \mathbf{u}} = 0$ . Since Eq. (72) depends only on the longitudinal component<sup>44</sup>  $\mathbf{u}_L$  (recall  $\nabla \cdot \mathbf{u}(\mathbf{r}) = \nabla \cdot \mathbf{u}_L(\mathbf{r})$ ), we can equivalently vary with respect to  $\mathbf{u}_L$ . Thus, we obtain the nontrivial ground-state distortion of a vortex lattice from the naive uniform (rigid-body) state in an inhomogeneous condensate characterized by the uniaxially symmetric superfluid density  $\rho_s(\mathbf{r}) = \rho_s(r)$ :

$$\mathbf{u}(\mathbf{r}) = -\frac{1}{8\omega \rho_s(r)} \nabla \left[ \rho_s(r) \ln \frac{c}{\xi^2 \omega(1 - \nabla \cdot \mathbf{u})} \right], \quad (73)$$

where  $c \equiv 1/e$ . For the case of  $\rho_s(r)$  largest at the center of the trap, the vortex distortion  $\mathbf{u}(\mathbf{r})$  is clearly in the outward radial direction and purely longitudinal for the case of an axially symmetric  $\rho_s(r)$ .

The nontrivial distortion  $\mathbf{u}(\mathbf{r})$  arises as a result of the competition between the vortex kinetic energy (second term in Eq. (72)), associated with vortex discreteness and the Magnus "energy" (first term in Eq. (72)). For a nonuniform  $\rho_s(r)$  the former is lowered by shifting vortices out to the condensate edge (along  $-\nabla \rho_s$ ), where  $\rho_s(r)$  and the associated kinetic energy cost is smaller. This is balanced by the Magnus force (which seeks to minimize the distortion  $\mathbf{u}(\mathbf{r})$ ) that is proportional to the difference between the vortex velocity  $\Omega \hat{\mathbf{z}} \times \mathbf{r}$  and the local superfluid velocity  $\bar{\mathbf{v}}_s(\mathbf{r}) = \Omega[\hat{\mathbf{z}} \times \mathbf{r} - 2\hat{\mathbf{z}} \times \mathbf{u}_L(\mathbf{r})]$ . Since for a weak distortion the former energy is linear and the latter is quadratic in  $\mathbf{u}(\mathbf{r})$ , a nontrivial vortex lattice distortion, given in Eq. (73), is always induced.

Using our main result for  $\mathbf{u}(\mathbf{r})$ , Eq. (73), the superfluid velocity can be easily computed using Eq. (66), giving

$$\bar{\mathbf{v}}_s(\mathbf{r}) \simeq \Omega \hat{\mathbf{z}} \times \left[ \mathbf{r} + \frac{1}{4\omega} \left( \ln \frac{c}{\xi^2 \omega} \right) \nabla \ln \rho_s \right], \quad (74)$$

where for simplicity we made an approximation  $\nabla \cdot \mathbf{u} \approx 0$  inside the logarithm of Eq. (73). Since typically  $\rho_s(r)$  is concave, largest at the center of trap and decreasing

monotonically with radius (although by tailoring a trap potential it can be made interestingly nonmonotonic; see Sec. VB 3 below), the superfluid velocity Eq. (74) is in fact *lower* than the rigid-body result by an amount that generically increases with radius. Thus, in the rotating (vortex lattice) frame the superfluid velocity is in the direction *opposite* to that of the imposed rotation (see Fig. 2).

Furthermore we note that, as illustrated in Fig. 2,  $\bar{\mathbf{v}}_s(\mathbf{r})$  in Eq. (74) exhibits radial shearing, namely the superfluid rotates with an  $r$ -dependent angular velocity and *not* simply as a rigid body with  $\bar{\mathbf{v}}_s(\mathbf{r}) = \Omega' \hat{\mathbf{z}} \times \mathbf{r}$  and  $\Omega' < \Omega$  (except in the case of Gaussian  $\rho_s(r)$ , see below).

A conventional fluid exhibiting such a radial shear past a conventional (e.g., colloidal) crystal would necessarily exert a viscous shear stress on the crystal, thereby inducing a helical-like shear strain  $\partial_r u_\phi$  ( $u_\phi$  an azimuthal lattice distortion) in the crystal. By symmetry arguments one would expect a similar helical (azimuthal radial-shear) distortion of the vortex lattice due to the shearing superfluid, in the direction opposite to the fluid flow. However, within our over-simplified ideal  $T = 0$  superfluid analysis (no normal, quasi-particle fluid), the forces on the vortex are purely radial (perpendicular to the superflow), and therefore only induce a radial (longitudinal) distortion, Eq. (73). Whether this intriguing, symmetry-suggested helical distortion of the vortex lattice will emerge from a more realistic (e.g., two-fluid model that includes thermally excited quasiparticles) calculation remains an interesting open question.

Using Eq. (73) together with Eq. (65) (i.e., taking the divergence of  $\mathbf{u}(\mathbf{r})$ ), or equivalently using Eq. (66) (i.e., taking the curl of  $\bar{\mathbf{v}}_s(\mathbf{r})$ ) we can compute the corresponding coarse-grained vortex density by solving the differential equation that  $\bar{n}_v(r)$  satisfies:

$$\bar{n}_v(r) = \frac{\omega}{\pi} + \frac{1}{8\pi} \nabla \cdot \left( \frac{1}{\rho_s(r)} \nabla [\rho_s(r) \ln \frac{c}{\pi \xi^2 \bar{n}_v(r)}] \right). \quad (75)$$

The physical picture embodied by Eq. (75) is straightforward to understand. The first term is the usual rigid body density discussed in the Introduction, corresponding to the vortex density in the limit of an infinite and homogeneous superfluid. Indeed, for uniform  $\rho_s(r)$ , Eq. (75) is *exactly* solved by the rigid-body vortex density (i.e.  $n_{v0} = \omega/\pi$ ), in agreement with Tkachenko's results<sup>17</sup>. The correction to  $n_{v0}$  (second term above) also vanishes in the dense vortex (or high-rotation rate,  $\bar{n}_v \xi^2 \approx 1$ ) limit<sup>15</sup>, as expected from the discussion in Sec. II A. Hence, consistent with experiments<sup>4,5,6,7,8,9</sup>, an approximately uniform rigid-body rotation corresponding to a constant vortex density  $n_{v0}$  is predicted even in the case of a spatially-varying superfluid density,  $\rho_s(r)$ . Consistent with earlier observations, since the condensate density variation in a trap is expected to satisfy  $\frac{\rho'_s(x)}{\rho_s(x)} \leq 0$ , Eq. (75) predicts that the coarse-grained vortex density is expected to be lower than the rigid body result  $n_{v0}$  by an amount that vanishes for a uniform superfluid.

For smooth variations in  $\rho_s(r)$ , we can replace  $\bar{n}_v(r)$  in the logarithm by its approximate value  $\omega/\pi$ , yielding our main result

$$\bar{n}_v(r) \approx \frac{\omega}{\pi} + \frac{1}{8\pi} \nabla \cdot \left( \frac{1}{\rho_s(r)} \nabla [\rho_s(r) \ln \frac{c}{\xi^2 \omega}] \right), \quad (76a)$$

$$\approx \frac{\omega}{\pi} + \bar{c} \nabla^2 \ln \rho_s(r), \quad (76b)$$

that relates vortex density to superfluid density, with

$$\bar{c} \equiv \frac{1}{8\pi} \ln \frac{c}{\xi^2 \omega}. \quad (77)$$

Because, as discussed in Sec. II, in the TF limit  $\rho_s(r)$  is simply determined by the trap profile with

$$\rho_s(r) \approx (\mu - V(r) + \frac{1}{2} m \Omega^2 r^2) / g, \quad (78)$$

Eq. (76a) gives an explicit prediction for the vortex density distribution in a rotating, inhomogeneous superfluid.

It is remarkable that, in the complementary lowest Landau level (LLL) limit, an identical relation (with the exception of the coefficient  $\bar{c}$ , which in the LLL regime is a pure number, independent of  $\xi$ ) emerges and was used by Ho<sup>45</sup> to argue (unfortunately incorrectly<sup>9</sup>, based on the observed approximate uniformity of the vortex lattice) for the Gaussian form of the condensate profile,  $\rho_s(r)$  in the LLL limit. In the recent work by Watanabe et al.<sup>18</sup>, a TF profile was found to be the optimal one in the LLL limit (in agreement with experiments<sup>9</sup>) leading these authors to assert (consistent with our earlier prediction<sup>11</sup>) that the vortex lattice is nonuniform in this regime. These latter findings were also supported by recent numerical solutions of the problem in the LLL regime<sup>19,46</sup>.

## B. Application to specific superfluid density profiles

We now apply our result for  $\bar{n}_v(r)$ , Eq. (75), to a variety of condensate profiles  $\rho_s(r)$ , realizable by tailoring the shape of the trap potential.

### 1. Gaussian $\rho_s(r)$

We first note that for the case of a Gaussian condensate profile Eq. (26), the differential equation for  $\bar{n}_v(r)$ , Eq. (75), is solved by a *uniform* density  $\bar{n}_{v,G}$  given by

$$\bar{n}_{v,G} = \frac{\omega}{\pi} - \frac{1}{4\pi R^2} \ln \frac{c}{\pi \xi^2 \bar{n}_{v,G}}, \quad (79a)$$

$$\approx \frac{\omega}{\pi} - \frac{1}{4\pi R^2} \ln \frac{c}{\xi^2 \omega}. \quad (79b)$$

This solution represents a perfect hexagonal lattice, static in the rotating frame, with a lattice constant

slightly larger than the rigid-body result. The corresponding superfluid velocity is given by the rigid-body form

$$\bar{\mathbf{v}}_s(\mathbf{r}) \approx \Omega' \hat{\mathbf{z}} \times \mathbf{r}, \quad (80)$$

with

$$\Omega' = \Omega \left( 1 - \frac{1}{4\omega R^2} \ln \frac{c}{\xi^2 \omega} \right), \quad (81)$$

slightly smaller than the imposed rotation frequency  $\Omega$ . This result, (derived within London approximation) is consistent with the prediction by Ho<sup>45</sup> (discussed above) of a Gaussian condensate profile for a uniform vortex lattice, derived in the complementary LLL regime. Because of the close similarity of this vortex configuration and the associated superflow to those of the rigid-body result, we expect difficulties for a direct experimental verification of our prediction in Eq. (79a) for the Gaussian condensate profile.

### 2. Inverted parabola $\rho_s(r)$ (harmonic trap)

For the most experimentally relevant case of a harmonic trap, (which, within the TF approximation, has the condensate profile  $\rho_s(r) \propto (R^2 - r^2)$  [c.f. Eq. (10)]), the vortex density profile Eq. (76a) reduces to the result advertised in Sec. I<sup>30</sup>:

$$\bar{n}_v(r) \simeq \frac{\omega}{\pi} - \frac{1}{2\pi} \frac{R^2}{(R^2 - r^2)^2} \ln \frac{c}{\xi^2 \omega}. \quad (82)$$

In Fig. 1 we plot Eq. (82) for experimentally realistic parameters  $\Omega = .86\Omega_t$ ,  $R = 49\mu m$  (top solid curve),  $\Omega = .57\Omega_t$ ,  $R = 31\mu m$  (middle solid curve),  $\Omega = .40\Omega_t$ ,  $R = 25\mu m$  (bottom solid curve) along with the rigid-body result (dashed curve) for the case of <sup>87</sup>Rb. Here,  $\xi$  is taken to be the TF value<sup>12,32</sup>

$$\xi = \frac{\hbar}{m\Omega_t R}, \quad (83)$$

and  $\Omega_t = 52s^{-1}$ . As illustrated in Fig. 13 our prediction for  $\bar{n}_v(r)$  compares well with the recent JILA data<sup>9</sup>. To obtain this fit, we used values for  $\Omega$  and  $R$  reported in Ref. 9, adjusting them (from  $\Omega/\Omega_t = .89$  and  $R = 50\mu m$ ) within the reported error bars ( $\pm 3$  and  $\pm 1\mu m$ , respectively) to find the best fit.

Equivalently, the above result predicts a hexagonal lattice constant ( $a(r) = (2/\sqrt{3}\bar{n}_v(r))^{1/2}$ ) that increases with  $r$ , as illustrated in Figs. 13 and 14, where in the former we again compare our theory with the JILA experiments (with the same data as in Fig. 1).

### 3. Nonmonotonic condensate profiles

It is clear that if the only variation of the condensate density is on the scale of the trap, Eq. (73) predicts a generically small (though observable<sup>9</sup>) distortion

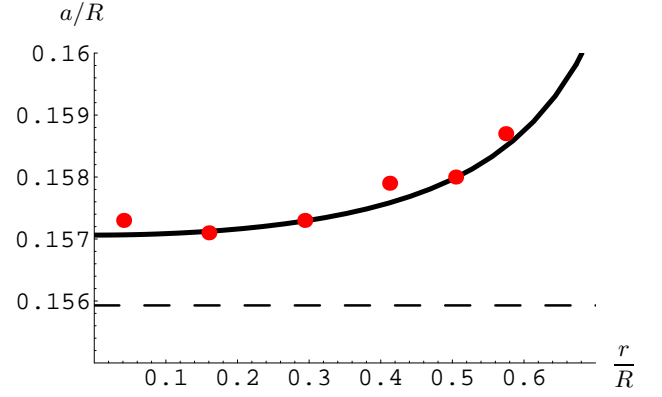


FIG. 13: (Color online) Plot of  $a/R$  (lattice spacing normalized to TF radius) as a function of radius using parameters  $\Omega/\Omega_t = .86$  and  $R = 49\mu m$ . Points are data adapted from Ref. 9. The dashed line is the rigid-body value of  $a/R$ .

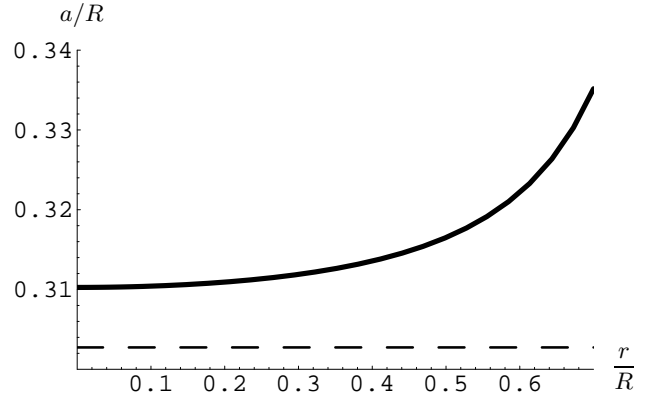


FIG. 14: Plot of  $a/R$  (lattice spacing normalized to TF radius) as a function of radius using parameters  $\Omega/\Omega_t = .57$  and  $R = 31\mu m$ . The dashed line is the rigid-body value of  $a/R$ .

of a uniform hexagonal vortex lattice that vanishes as  $\nabla^2 \ln \rho_s(r) \sim 1/R^2$  (for  $r \ll R$ ). To the extent that observed lattices (see, e.g., Refs. 4,5,6,7,8,9) are remarkably uniform, this is a required success of our theory. However, to more stringently test our predictions, in the present section we calculate vortex lattice distortions for nonmonotonic (but still uniaxial) condensate density profiles  $\rho_s(r)$  that also vary on a scale smaller than the condensate's overall size  $R$ . We expect that such  $\rho_s(r)$  can be experimentally realized by confining a condensate inside a nonmonotonic trap potential  $V(r)$  tailored by adjusting a combination of magnetic and optical fields.

For simplicity, ignoring the weak variation of the vortex density inside the argument of the logarithm, i.e., replacing  $1 - \nabla \cdot \mathbf{u}$  by unity, the distortion away from a hexagonal rigid-body array (which is a hexagonal lattice with lattice parameter  $(2/\sqrt{3}n_{v0})^{1/2}$ ) is given by

$$\mathbf{u}(\mathbf{r}) \simeq -\frac{\nabla \rho_s(r)}{8\omega \rho_s(r)} \ln \frac{c}{\xi^2 \omega}. \quad (84)$$

We first consider perhaps the simplest nonmonotonic condensate profile with a dip in its center of spatial extent

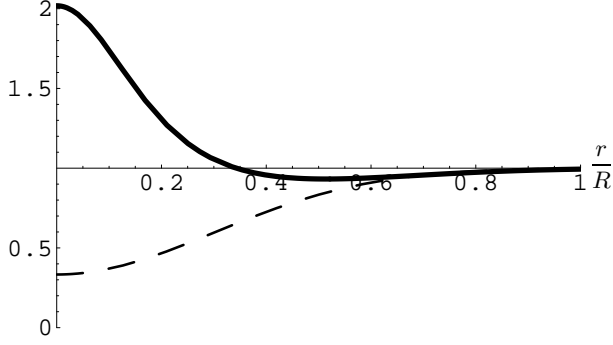


FIG. 15: Main: The solid line depicts the vortex density  $\bar{n}_v(r)/n_{v0}$  as a function of radius for the condensate profile Eq. (85). The dashed line plots  $\rho_s(r)/\rho_0$ .

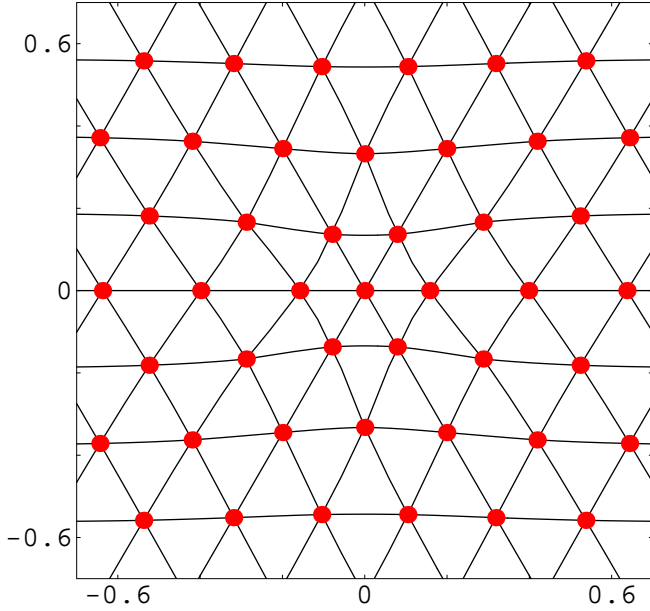


FIG. 16: (Color online) Distorted vortex lattice (points) arising from the condensate profile Eq. (85) containing a depletion near the origin with lines to guide the eye.

$\ell$ , that we model by

$$\rho_s(r) = \rho_0 - \rho_1 \exp(-r^2/2\ell^2), \quad (85)$$

with  $\rho_1 < \rho_0$ , where the finite asymptotic density  $\rho_0$  is strictly speaking not a constant but varies on a much larger scale  $R$  and is determined by an overall large-scale trap with  $R \gg \ell$ . A qualitatively similar condensate profile can be generated by a “Mexican hat”-like trap potential, as experimentally demonstrated by the research groups of Dalibard<sup>8</sup> and Ketterle<sup>47</sup>. Using such  $\rho_s(r)$

inside Eq. (73) and Eq. (75) we find

$$\mathbf{u}(\mathbf{r}) = -\frac{1}{8\omega\ell^2} \ln \frac{c}{\xi^2\omega} \frac{\rho_0}{\rho_1} \frac{\mathbf{r}}{\exp(\frac{r^2}{2\ell^2}) - 1}, \quad (86a)$$

$$\bar{n}_v(r) = \frac{\omega}{\pi} + \frac{1}{8\pi\ell^2} \ln \frac{c}{\xi^2\omega} \left[ \frac{2}{\frac{\rho_0}{\rho_1} \exp(r^2/2\ell^2) - 1} - \frac{r^2}{\ell^2} \frac{\frac{\rho_0}{\rho_1} \exp(r^2/2\ell^2)}{(\frac{\rho_0}{\rho_1} \exp(r^2/2\ell^2) - 1)^2} \right]. \quad (86b)$$

We plot the corresponding vortex density Eq. (86b) in Fig. 15 for a large slowly-rotating condensate of <sup>87</sup>Rb atoms with parameters ( $R = 500\mu\text{m}$ ,  $\Omega = 0.2\text{s}^{-1}$ ,  $\rho_1/\rho_0 = 0.67$ , and  $\ell = 0.3R$ ) that are slightly different than typical values of present-day experiments to enhance visualization of the distortion. Consistent with our earlier qualitative discussion,  $\bar{n}_v(r)$  is largest where  $\rho_s(r)$  is smallest. Near  $r = .5R$ ,  $\bar{n}_v(r)$  actually drops below its rigid-body value. The corresponding distortion  $\mathbf{u}(\mathbf{r})$  of the vortex lattice is illustrated in Fig. 16, showing vortices displacing against the local gradient in  $\rho_s(r)$ .

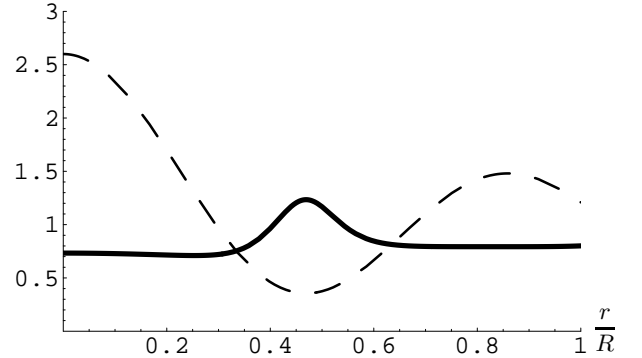


FIG. 17: Plot of condensate profile  $\rho_s(r)/\rho_0$  (dashed line) and vortex density  $\bar{n}_v(r)/n_{v0}$  (solid line) for the oscillatory profile Eq. (87) with parameters  $R = 49\mu\text{m}$  and  $\ell = 6\mu\text{m}$ .

Since  $\mathbf{u}(\mathbf{r})$  is constrained to vanish at the trap center where  $\nabla\rho_s = 0$  (see Eq. (84)), to maximize the distortions associated with a spatially-varying  $\rho_s(r)$  it makes sense to consider a condensate profile that exhibits its most rapid variation away from this symmetry point, i.e., at nonzero radii. Motivated by this we consider a trap potential and therefore a condensate density that oscillates with  $r$ . For concreteness we model such  $\rho_s(r)$  with a Bessel function

$$\rho_s(r) = \rho_0 + \rho_1 J_0(r/\ell), \quad (87)$$

with  $\ell$  characterizing the length-scale of the oscillations and  $\rho_0$  (as in the previous example) weakly  $r$  dependent on a much larger overall trap scale  $R$ , with  $R \gg \ell$ . To keep the overall condensate density positive we choose  $\rho_1 < 2.48\rho_0$ . For this condensate profile (displayed in Fig. 17, dashed curve) we compute the resulting vortex density  $\bar{n}_v(r)$  and illustrate it in Fig. 17 (solid curve)



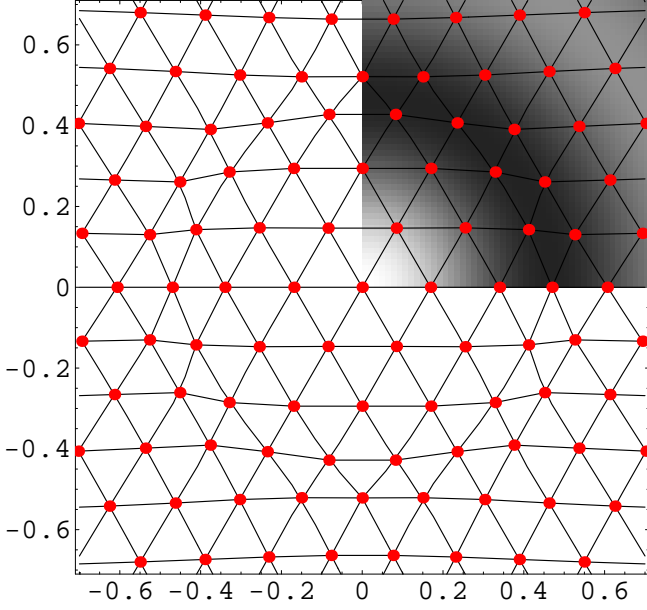


FIG. 18: (Color online) Vortex positions (measured relative to  $R$ ) for the profile Eq. (87) with lines to guide the eye. The parameters  $R = 49\mu m$  and  $\ell = 6\mu m$ . For the upper right quadrant, we have shown a density plot of  $\rho_s(r)$  with the light areas denoting regions of high  $\rho_s$ .

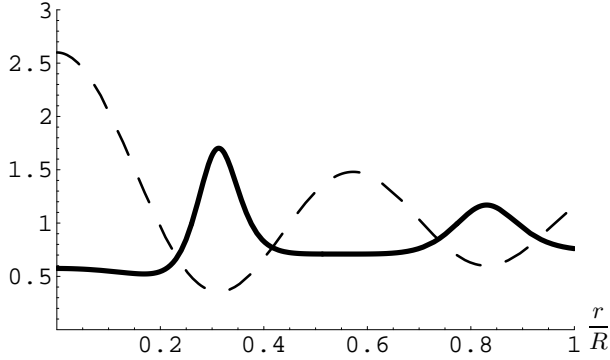


FIG. 19: Plot of condensate profile  $\rho_s(r)/\rho_0$  (dashed line) and vortex density  $\bar{n}_v(r)/n_{v0}$  (solid line) for the oscillatory profile Eq. (87) with parameters  $R = 49\mu m$  and  $\ell = 4\mu m$ .

for parameters (TF radius  $R = 49\mu m$ , trap frequency  $\Omega_t = 52s^{-1}$ ,  $\ell = 6\mu m$ ,  $\rho_1/\rho_0 = 1.6$ ,  $\Omega/\Omega_t = .86$  and with  $\xi$  given by Eq. (83)) that are consistent with recent Rb experiments at JILA<sup>7,9</sup>. At the location of the dip in the condensate density ( $r \approx 0.5R$ ),  $\bar{n}_v(r)$  exhibits a corresponding maximum. The effect on the locations of the vortices is quite striking, as shown in Fig. 18: the vortex rings near the dip are compressed together. In the upper right quadrant we have included a density plot of  $\rho_s(r)$  to show how regions of low  $\rho_s(r)$  (which are darker) induce higher local vortex density. Thus, this profile nicely illustrates the principle that vortices migrate to regions

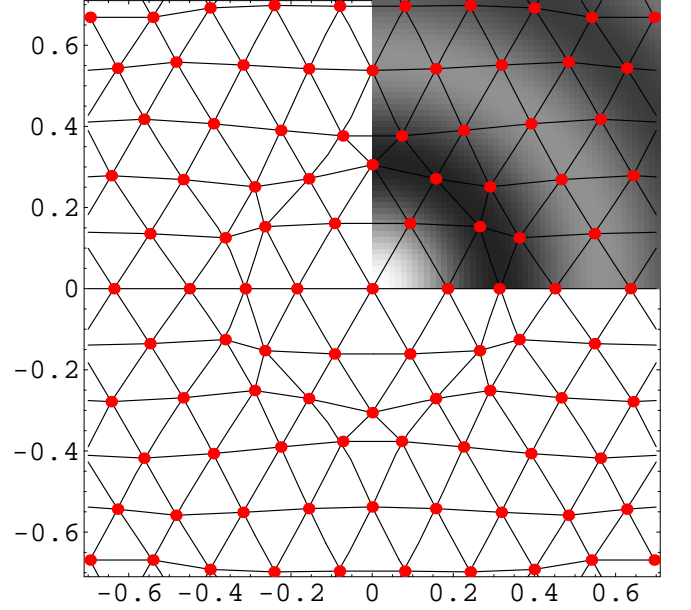


FIG. 20: (Color online) Vortex positions (measured relative to  $R$ ) for the profile Eq. (87) with lines to guide the eye. The parameters  $R = 49\mu m$  and  $\ell = 4\mu m$ . For the upper right quadrant, we have shown a density plot of  $\rho_s(r)$  with the light areas denoting regions of high  $\rho_s$ .

where  $\rho_s$  is small to lower the kinetic energy.

The case of a smaller value of  $\ell$  ( $\ell = 4\mu m$ ), such that  $\rho_s(r)$  has two minima before  $r = R$  is reached, is illustrated in Figs. 19 and 20, again demonstrating how (as expected) vortices congregate near radial minima of  $\rho_s(r)$ , with a local density and superfluid velocity that actually *exceed* their rigid-body values.

### C. Effect of inhomogeneous vortex density on condensate profile

Thus far, to calculate the average vortex density  $\bar{n}_v(r)$  we have used the TF expression for the condensate density  $\rho_s(\mathbf{r})$ , Eq. (9), that was derived in Sec. II within an approximation of a rigid-body superflow profile. However, as we have shown in the previous section, the superflow profile is itself modified inside an inhomogeneous condensate. Hence in principle we need to determine  $\bar{n}_v(r)$  and  $\rho_s(r)$  by self-consistently solving the coupled equations Eq. (8) and Eq. (75), together with  $\bar{n}_v(r) = \frac{m}{2\pi\hbar} \nabla \times \bar{\mathbf{v}}_s$ . However, as we show below, for a smooth trap potential, to a good approximation, the effect of the inhomogeneity of the vortex distribution on the equilibrium  $\rho_s(r)$  is negligible, with corrections vanishing as a higher power in  $\nabla \rho_s/\rho_s \sim 1/R$ .

To show this, we repeat the steps of Sec. V A, but now using the full bosonic energy density Eq. (7) instead of keeping only the  $\theta$ -dependent terms (i.e. as in Eq. (68)).

This gives:

$$E \simeq \frac{\hbar^2}{2m} \int d^2r \rho_s(\mathbf{r}) \left[ \pi \bar{n}_v \ln \frac{1}{\pi \xi^2 \bar{n}_v} + 4\omega^2 u_L(\mathbf{r})^2 \right] + \int d^2r \left[ \left( V - \frac{1}{2} m \Omega^2 r^2 - \mu \right) \rho_s(\mathbf{r}) + \frac{g}{2} \rho_s(\mathbf{r})^2 \right], \quad (88)$$

where we remind the reader that  $\bar{n}_v$  is related to  $\mathbf{u}_L$  via Eq. (65), and, in the spirit of the TF approximation, we have still neglected the subdominant (away from the condensate edge,  $r \ll R$ )  $\nabla \rho_s$  contributions to the energy. The corresponding, coupled Euler-Lagrange equations ( $\delta E / \delta u_L = 0$ ,  $\delta E / \delta \rho_s = 0$ ) that determine  $\bar{n}_v(\mathbf{r})$  (through  $\mathbf{u}_L$ ) and  $\rho_s(\mathbf{r})$  are given by:

$$\mathbf{u}_L(\mathbf{r}) = -\frac{1}{8\omega} \frac{\nabla \rho_s(r)}{\rho_s(r)} \ln \frac{c}{\xi^2 \omega}, \quad (89a)$$

$$\rho_s(\mathbf{r}) = \frac{1}{g} \left[ \mu - b \hbar \Omega - \left( V(r) - \frac{1}{2} m \Omega^2 r^2 \right) - \frac{1}{g} \left[ 2m \Omega^2 u_L^2 - \hbar \Omega \nabla \cdot \mathbf{u} \ln \frac{1}{\xi^2 \omega} \right] \right], \quad (89b)$$

where, as before, in Eq. (89a) we have replaced  $1 - \nabla \cdot \mathbf{u} \simeq 1$  in the argument of the logarithm of Eq. (73), and defined a parameter  $b \equiv \frac{1}{2} \ln \frac{1}{\xi^2 \omega}$ . While the equation for  $u_L$  remains unchanged, the equation for  $\rho_s(\mathbf{r})$  is modified by the vortex kinetic energy, that, as expected, suppresses it.

Although these coupled equations are in general quite nontrivial, for a smooth trap the distortion  $\mathbf{u}(\mathbf{r})$  is small, vanishing with  $\nabla \rho_s / \rho_s \sim 1/R$ . Hence, they can be straightforwardly solved by iteration in this small parameter. To lowest order we can simply neglect the vortex lattice distortion  $\mathbf{u}(\mathbf{r})$  inside the  $\rho_s(\mathbf{r})$  equation, obtaining our previous symmetric TF result

$$\rho_s(r) \approx \frac{1}{g} \left[ \mu - b \hbar \Omega - \frac{1}{2} m (\Omega_t^2 - \Omega^2) r^2 \right], \quad (90)$$

corrected only by  $b \hbar \Omega$ , that is small compared to  $\mu$ . Higher order corrections to  $\rho_s(r)$  are easily obtained by an iterative procedure, thereby generating a perturbative expansion in  $1/R$ . Hence, in the high rotation limit,  $\Omega \rightarrow \Omega_t$  (corresponding to a divergent  $R(\Omega)$ , Eq. (11)) the TF condensate density profile Eq. (9) is an accurate description, in agreement with recent results obtained within the lowest Landau level approximation<sup>18,19</sup>.

## VI. ELASTIC THEORY AND TKACHENKO MODES

Having determined the equilibrium vortex distribution in a spatially inhomogeneous rotating condensate, we

now study long-wavelength vortex fluctuations about this slightly inhomogeneous equilibrium vortex state. To this end we derive a vortex lattice elastic energy by expanding the total energy Eq. (72) to harmonic order in small distortions  $\boldsymbol{\epsilon}(\mathbf{r})$  about the ground-state configuration  $\mathbf{u}_0(\mathbf{r})$  [satisfying Eq. (73)], defined by  $\mathbf{u}(\mathbf{r}) = \mathbf{u}_0(\mathbf{r}) + \boldsymbol{\epsilon}(\mathbf{r})$ . We find

$$E_{el}[\boldsymbol{\epsilon}(\mathbf{r})] = \frac{\hbar^2}{2m} \int d^2r \rho_s(r) \left[ 4\omega^2 \epsilon_L^2 - \frac{\omega}{2} \frac{(\nabla \cdot \boldsymbol{\epsilon})^2}{1 - \nabla \cdot \mathbf{u}_0} \right], \quad (91a)$$

$$\simeq \frac{\hbar^2}{2m} \int d^2r \rho_s(r) \left[ 4\omega^2 \epsilon_L^2 - \frac{\omega}{2} (\nabla \cdot \boldsymbol{\epsilon})^2 \right], \quad (91b)$$

where in Eq. (91b) we have approximated  $\mathbf{u}_0 \simeq 0$ .

This compressional energy must be augmented by the elastic energy of the vortex lattice *shear* deformation, that is clearly missed at this level of a coarse-grained (density-functional) approximation. We follow Baym and Chandler<sup>42</sup> and fix the shear modulus using Tkachenko's<sup>17,48</sup> exact result for the uniform condensate, that we expect (given the high uniformity of the vortex lattice observed in experiments and demonstrated here analytically) to be a good approximation even for our case of a spatially-varying  $\rho_s(r)$ . This yields

$$E_{el} \simeq \frac{\hbar^2}{2m} \int d^2r \rho_s(r) \left[ 4\omega^2 \epsilon_L^2 - \frac{\omega}{2} (\nabla \cdot \boldsymbol{\epsilon})^2 + \frac{\omega}{4} \left( \frac{\partial \epsilon_x}{\partial x} - \frac{\partial \epsilon_y}{\partial y} \right)^2 + \frac{\omega}{4} \left( \frac{\partial \epsilon_x}{\partial y} + \frac{\partial \epsilon_y}{\partial x} \right)^2 \right]. \quad (92)$$

The dynamics of long-wavelength elastic vortex fluctuations is governed by the balance of the Magnus “force” against the “elastic” force associated with the distortion  $\boldsymbol{\epsilon}(\mathbf{r}, t)$  of the vortex lattice

$$-\frac{\pi}{\omega} \frac{\delta E_{el}}{\delta \boldsymbol{\epsilon}(\mathbf{r}, t)} + 2\pi \hbar \rho_s \hat{\mathbf{z}} \times \dot{\boldsymbol{\epsilon}}(\mathbf{r}, t) = 0, \quad (93)$$

where  $\dot{\boldsymbol{\epsilon}} \equiv \frac{d\boldsymbol{\epsilon}}{dt}$  and the inverse of the average vortex density factor  $1/n_{v0} = \pi/\omega$  arises from the Jacobian relating the variation with respect to  $\mathbf{r}_i$  to the functional variation with respect to  $\boldsymbol{\epsilon}(\mathbf{r}_i)$ . Carrying out the functional derivative yields the following equation for  $\boldsymbol{\epsilon}(\mathbf{r}, t)$ :

$$\rho_s \hat{\mathbf{z}} \times \dot{\boldsymbol{\epsilon}} = -\frac{2\hbar\omega}{m} \nabla \int d^2\mathbf{r}' \rho_s(r') \boldsymbol{\epsilon}_L(\mathbf{r}', t) \cdot \nabla G(\mathbf{r}' - \mathbf{r}) - \frac{\hbar}{8m} ([\nabla \rho_s \cdot \nabla] \boldsymbol{\epsilon} + [\hat{\mathbf{z}} \cdot (\nabla \rho_s \times \nabla)] \hat{\mathbf{z}} \times \boldsymbol{\epsilon} + \rho_s \nabla^2 \boldsymbol{\epsilon} - 2 \nabla [\rho_s \nabla \cdot \boldsymbol{\epsilon}]). \quad (94)$$

A full solution of Eq. (94) is beyond the scope of this paper and we leave it for future research. In spite of its complexity it is reassuring that for a uniform condensate ( $r$ -independent  $\rho_s$ ) the divergence and curl of Eq. (94) are equivalent to Eqs. (71) and (72) of Ref. 42, respectively. In the following, we proceed by making a simple analytic approximation to Eq. (94) to bring out the leading order effect of the condensate inhomogeneity on the Tkachenko waves.

For long-wavelength Tkachenko modes, with  $\frac{1}{a} \gg k \gtrsim \frac{1}{R}$ , it is clear that the first term on the right side of Eq. (94) (which is purely longitudinal) dominates over the second since  $\omega \propto 1/a^2$ . Taking the divergence of both sides of Eq. (94) and neglecting the subdominant second term, we find

$$\nabla \times \dot{\boldsymbol{\epsilon}} = -2\Omega \nabla \cdot \boldsymbol{\epsilon} \hat{\mathbf{z}}, \quad (95)$$

to leading order in a double expansion in spatial derivatives of  $\boldsymbol{\epsilon}$  and  $\rho_s$ . The transverse part of Eq. (94) is obtained by taking its curl, which leads to

$$\begin{aligned} \nabla \times [\rho_s \hat{\mathbf{z}} \times \dot{\boldsymbol{\epsilon}}] &= -\frac{\hbar}{8m} \left[ \nabla \times (\rho_s \nabla^2 \boldsymbol{\epsilon}) \right. \\ &\quad \left. + \nabla \times ([\nabla \rho_s \cdot \nabla] \boldsymbol{\epsilon} + [\hat{\mathbf{z}} \cdot (\nabla \rho_s \times \nabla)] \hat{\mathbf{z}} \times \boldsymbol{\epsilon}) \right]. \end{aligned} \quad (96)$$

Henceforth, for simplicity, we restrict our attention to the case of a Gaussian  $\rho_s(r)$ , Eq. (26), which satisfies  $\nabla \rho_s(r) = -\mathbf{r} \rho_s(r)/R^2$ . To leading order in spatial gradients, the quantity in parentheses in the second line of Eq. (96) reduces to

$$[\nabla \rho_s \cdot \nabla] \boldsymbol{\epsilon} + [\hat{\mathbf{z}} \cdot (\nabla \rho_s \times \nabla)] \hat{\mathbf{z}} \times \boldsymbol{\epsilon} \simeq \frac{\rho_s \boldsymbol{\epsilon}}{R^2}. \quad (97)$$

Inserting Eq. (97) into Eq. (96) and expanding the result to leading order in derivatives of  $\rho_s$ , we have

$$\nabla \cdot \dot{\boldsymbol{\epsilon}} \hat{\mathbf{z}} \simeq -\frac{\hbar}{8mR^2} \nabla \times \boldsymbol{\epsilon} - \frac{\hbar}{8m} \nabla^2 (\nabla \times \boldsymbol{\epsilon}), \quad (98)$$

where we have used  $\nabla \times \nabla^2 \boldsymbol{\epsilon} = \nabla^2 (\nabla \times \boldsymbol{\epsilon})$ . Combining this result with Eq. (95), we finally obtain an equation for the transverse vortex fluctuations  $\nabla \times \boldsymbol{\epsilon}$ :

$$\frac{d^2}{dt^2} (\nabla \times \boldsymbol{\epsilon}) = \frac{\hbar\Omega}{4m} \left( \frac{1}{R^2} + \nabla^2 \right) (\nabla \times \boldsymbol{\epsilon}). \quad (99)$$

The spatial and temporal Fourier transform of this linear wave equation then immediately gives the Tkachenko mode dispersion  $\Omega_T(k)$ :

$$\Omega_T(k) = \sqrt{\hbar\Omega/4m} \sqrt{k^2 - R^{-2}}, \quad (100)$$

that, in the uniform limit  $R \rightarrow \infty$ , recovers the standard linear dispersion result  $\Omega_T(k) = k\sqrt{\hbar\Omega/4m}$  (see Refs. 42,48). Given the small gradient in  $\rho_s(r)$  expansion that led to this result, the wavevector is obviously limited to the physically sensible range  $1/a > k > 1/R$ . No doubt a more detailed analysis of Eq. (94) is needed to obtain a more accurate prediction for Tkachenko eigenmodes and their dispersion in an inhomogeneous condensate characterized by a generic condensate profile  $\rho_s(r)$ . We leave such analysis, as well as an extension of Eq. (94) that includes condensate *density* fluctuations, as discussed in the recent work by Baym<sup>49</sup> (see also Ref. 50), to future research.

## VII. SUMMARY AND CONCLUSIONS

To summarize, we have presented a London theory of a vortex state in an inhomogeneous rotating Bose-Einstein condensate. Our most important result (Eq. (75)) is the relation between the vortex density  $\bar{n}_v(r)$  and the superfluid density  $\rho_s(r)$ . When applied to a harmonic trap, this result provides a simple explanation for the observed highly regular vortex arrays in such strongly inhomogeneous condensates, and the observed Thomas-Fermi parabolic condensate profile. This relation also predicts a slight inhomogeneity in the vortex spatial distribution, that has recently (since our prediction) been observed in experiments and simulations from JILA<sup>9</sup>. As we discussed in the main text, this relation between  $\bar{n}_v(r)$  and  $\rho_s(r)$  can be more stringently tested by studying vortex lattice distortions induced by nonmonotonic condensate profiles, tailored with various trapping potentials.

As an important digression, we also studied the superflow in the vicinity of an isolated vortex, calculating the superfluid velocity distortion induced by a spatially-varying condensate. The associated additional contribution to the superflow is directed orthogonal to the displacement of the vortex away from the trap center, thereby providing a simple explanation for precession of such vortices about the trap center with radially-independent frequency.

With respect to our vortex lattice result, it is important to stress that our prediction of the deviation of the vortex density from the spatially independent (rigid-body) result is more than just a suppression of the total vortex number (a somewhat trivial and experimentally difficult<sup>51</sup> effect to detect, that follows directly from the existence of  $\Omega_{c1}$ , as can be seen from arguments in Sec. II B and Fig. 4). In particular, it is not a simple surface effect, such as, e.g., a missing vortex ring at the edge of the condensate, as for example observed in simu-

lations of Feder and Clark<sup>12</sup> and predicted theoretically for uniform superfluids some time ago<sup>52</sup>.

Our prediction of a radially increasing vortex lattice spacing across the *bulk* of a condensate (that does not require a precise measure of  $\Omega$ <sup>51</sup>), shows quantitative agreement with recent JILA data<sup>9</sup>, exhibiting the same  $\sim 2\%$  lattice distortion.

We conclude by noting that a number of important extensions of our work remain. Based on symmetry considerations we have suggested that an azimuthally directed vortex lattice radial-shear distortion  $\partial_r u_\phi$  will be induced by the radially-shearing superfluid. Clearly, it is important to determine theoretically whether such interesting chiral vortex lattice distortion is indeed present. This should be possible to assess within either a two-fluid hydrodynamic model or by incorporating thermally-excited Bogoliubov quasi-particles into our theory. A more careful treatment of vortex discreteness (that goes beyond our simple density-functional-like approximation), from which a finite vortex lattice shear modulus must emerge is also highly desirable. This would allow a first-principles treatment of Tkachenko modes, that is more precise than that presented here. Finally, the extension of our work to three dimensions, where a nontrivial  $z$ -dependence of the vortex-line density profile is expected, is another important future direction.

### Acknowledgments

We gratefully acknowledge useful discussions with A. Andreev, I. Coddington, E. Cornell, P. Engels, A. Fetter and V. Schweikhard as well as support from NSF DMR-0321848 and the Packard Foundation.

### APPENDIX A: VORTEX PRECESSION IN A UNIFORM SUPERFLUID

Our derivation in Sec. IV of vortex precession in an inhomogeneous trapped superfluid can be complemented

by an exact calculation of vortex precession in a *homogeneous* condensate confined to a finite “bucket” of radius  $R$  (see Ref. 24). To model this system we take  $\rho_s$  be a constant  $\rho_0$  for  $r < R$  and zero for  $r > R$ . For this case, the single-vortex problem is solved by the method of images to enforce the boundary condition of no outward current (i.e.  $\nabla\theta$  must be orthogonal to the boundary)<sup>35</sup>.

It is straightforward to verify that a single vortex at  $\mathbf{r}_0$  in the bucket geometry has the solution

$$\nabla\theta(\mathbf{r}) = \frac{\hat{\mathbf{z}} \times (\mathbf{r} - \mathbf{r}_0)}{(\mathbf{r} - \mathbf{r}_0)^2} - \frac{\hat{\mathbf{z}} \times (\mathbf{r} - \mathbf{r}_i)}{(\mathbf{r} - \mathbf{r}_i)^2}, \quad (\text{A1})$$

where  $\mathbf{r}_i = \mathbf{r}_0 R^2/r_0^2$  is the “image charge”. Thus, although the condensate is homogeneous in the bulk, the nontrivial boundary condition necessarily introduces a curl-free (in the bulk) correction  $\nabla\theta_a$  to the superflow (second term in Eq. (A1)), that has a similar physical effect as that due to the bulk condensate inhomogeneity studied in Sec. IV.

As for an inhomogeneous condensate, the background superflow at the vortex and thus the vortex dynamics are entirely determined by the image charge term. Evaluating the associated contribution at  $\mathbf{r}_0$  and using Eq. (47) we find

$$\dot{\mathbf{r}}_0 = \frac{\hbar}{m} \frac{\hat{\mathbf{z}} \times \mathbf{r}_0}{R^2 - r_0^2}, \quad (\text{A2})$$

showing that a vortex located off-center in a finite “bucket” will precess about the origin in a sense similar to that embodied in Eq. (48) and Eq. (52), with the frequency near the center of order  $\hbar/mR^2$ , corresponding to a unit of angular momentum for a boson at the boundary of the condensate, as found for an inhomogeneous condensate.

<sup>1</sup> L. Onsager, Nuovo Cim. Suppl. 2 **6**, 279 (1949).

<sup>2</sup> R.P. Feynman, in *Progress in Low Temperature Physics*, C.J. Gorter, ed. (1955).

<sup>3</sup> M.R. Matthews, B.P. Anderson, P.C. Haljan, D.S. Hall, C.E. Wieman and E.A. Cornell, Phys. Rev. Lett. **83**, 2498 (1999).

<sup>4</sup> K.W. Madison, F. Chevy V. Bretin and J. Dalibard, Phys. Rev. Lett. **86**, 4443 (2001).

<sup>5</sup> J.R. Abo-Shaeer, C. Raman, J.M. Vogels and W. Ketterle, Science **292**, 476 (2001).

<sup>6</sup> P.C. Haljan, I. Coddington, P. Engels and E.A. Cornell, Phys. Rev. Lett. **87**, 210403 (2001).

<sup>7</sup> P. Engels, I. Coddington, P.C. Haljan, V. Schweikhard and E.A. Cornell, Phys. Rev. Lett. **90**, 170405 (2003).

<sup>8</sup> Vincent Bretin, Sabine Stock, Yannick Seurin and Jean Dalibard, Phys. Rev. Lett. **92**, 050403 (2004).

<sup>9</sup> I. Coddington, P.C. Haljan, P. Engels, V. Schweikhard, S. Tung and E.A. Cornell, cond-mat/0405240.

<sup>10</sup> J.R. Anglin and M. Crescimanno, cond-mat/0210063.

<sup>11</sup> Daniel E. Sheehy and Leo Radzihovsky, cond-mat/0402637.

<sup>12</sup> David L. Feder and Charles W. Clark, Phys. Rev. Lett., **87**, 190401 (2001).

<sup>13</sup> In superconductors, vortex pinning by  $\rho_s(r)$  inhomogeneities is due to the lowering of the loss of condensation energy (i.e. an increase in condensation energy) when the “normal” vortex core spatially coincides with the material inhomogeneity. Because vortex motion generates electric

fields (Josephson relation), vortex pinning is in fact crucial for type-II superconductivity.

- <sup>14</sup> For our purposes here, it is sufficient to confine our analysis to a zero-temperature mean-field approximation. At this level, for weak interactions appropriate for a dilute gas the condensate depletion is vanishingly small, allowing us to ignore the distinction between the superfluid density  $\rho_s(r)$  and the condensate density  $|\Phi(r)|^2$ .
- <sup>15</sup> In this article we do not consider the extremely high rotation rate regime, where Landau level quantization is important, boson and vortex densities are comparable and therefore vortices must again be treated as discrete and furthermore as quantum mechanical objects. Even for a large filling fraction  $N_b/N_v$  so that the rotated superfluid remains a well-ordered vortex lattice, for sufficiently weak interactions, low density and large rotation rate, the coherence length grows to become comparable to inter-vortex spacing, invalidating our London approximation. The many-body ground state is then still well-described by a product of single-particle vortex-lattice wavefunctions (all bosons occupying this same vortex state), but (unlike in London approximation) in this so-called lowest Landau level (LLL) regime, constructed as a superposition of orbitals constrained to the LLL. As argued theoretically<sup>16</sup> and demonstrated convincingly experimentally<sup>9</sup>, within this high rotation LLL regime, the  $\omega\xi^2 \propto (\xi/a)^2$  saturates, approaching a constant.
- <sup>16</sup> Gordon Baym and C.J. Pethick cond-mat/0308325.
- <sup>17</sup> V.K. Tkachenko, Zh. Eksp. Teor. Fiz. **49**, 1875 (1965) [Sov. Phys. JETP **22**, 1282 (1966)].
- <sup>18</sup> Gentaro Watanabe, Gordon Baym and C.J. Pethick, cond-mat/0403407.
- <sup>19</sup> N.R. Cooper, S. Komineas and N. Read, cond-mat/0404112.
- <sup>20</sup> B.Y. Rubinstein and L.M. Pismen, Physica D **78**, 1 (1994); see also L.M. Pismen *Vortices in Nonlinear fields*, Oxford (1999).
- <sup>21</sup> P.O. Fedichev and G.V. Shlyapnikov, Phys. Rev. A **60**, 1779 (1999).
- <sup>22</sup> Marion Linn and Alexander L. Fetter, Phys. Rev. A **61**, 063603 (2000).
- <sup>23</sup> Emil Lundh and P. Ao, Phys. Rev. A **61**, 063612 (2000).
- <sup>24</sup> S.A. McGee and M.J. Holland, Phys. Rev. A, **63**, 043608 (2001).
- <sup>25</sup> Anatoly A. Svidzinsky and Alexander L. Fetter, Phys. Rev. Lett. **84**, 5919 (2000); Phys. Rev. A **62**, 063617 (2000).
- <sup>26</sup> J.R. Anglin, Phys. Rev. A **65**, 063611 (2002).
- <sup>27</sup> The result for the superfluid velocity near an off-axis vortex, that we find here, was first published in Ref. (20) and generalized to the three-dimensional case in Ref. (25). However, to the best of our knowledge, the extension of the solution for  $\mathbf{v}_s(r)$  to the region outside the immediate vicinity of the vortex has not appeared in the literature until our work<sup>11</sup>.
- <sup>28</sup> B.P. Anderson, P.C. Haljan, C.E. Wieman and E.A. Cornell, Phys. Rev. Lett. **85**, 2857 (2000).
- <sup>29</sup> The energy density for the Bose condensate can be straightforwardly obtained from a standard interacting boson Hamiltonian, with boson operators approximated by a classical condensate field, appropriate for the BEC state. Equivalently, the same result can be obtained from a mean-field approximation to the coherent state path integral for the partition function for the interacting boson problem.
- <sup>30</sup> This is what is known as the Thomas-Fermi approximation, which ignores the kinetic energy (i.e. gradients in the condensate wavefunction) in comparison to the trap potential and boson interactions and which is valid away from the condensate edges. Not surprisingly, this neglect of kinetic energy leads to unphysical anomalies near the condensate edges such as divergent corrections to the vortex density  $\bar{n}_v(r)$  as  $r \rightarrow R$ . Although in a more careful approximation these divergences do not appear, we expect that our small gradient (in  $\ln \rho_s(r)$ ) analysis breaks down near the edge of the condensate, where the corrections to the uniform vortex density and rigid-body superfluid velocity are large.
- <sup>31</sup> See, e.g., A.J. Leggett, Rev. Mod. Phys. **71**, S318 (1999).
- <sup>32</sup> Gordon Baym and C.J. Pethick, Phys. Rev. Lett. **76**, 6 (1996).
- <sup>33</sup> We must remark that, since  $N$  is a discrete variable, in actuality one expects steps in  $N$  as a function of  $\Omega$  (see, e.g., Fig 2 of Ref. 34) which become negligible at large  $\Omega$ .
- <sup>34</sup> D.A. Butts and D.S. Rokhsar, Nature (London) **397**, 327 (1999).
- <sup>35</sup> In fact, for a vortex in a *finite* but *homogeneous* superfluid (e.g., helium in a “bucket”, for which the superfluid density is finite at the boundary, vanishing only over an atomic length scale), the vanishing-current boundary condition is crucial for obtaining the correct single-vortex energy and dynamics (e.g., the precession of an off-axis vortex). These are strongly affected by the interaction of the vortex with its image vortex introduced to enforce the above boundary condition.
- <sup>36</sup> S. Inouye, S. Gupta, T. Rosenband, A.P. Chikkatur, A. Górlitz, T.L. Gustavson, A.E. Leanhardt, D.E. Pritchard and W. Ketterle, Phys. Rev. Lett. **87**, 080402 (2001).
- <sup>37</sup> This is up to a curl-free vector field  $V(r, \phi)\hat{\phi}$ , with  $V(r, \phi)$  chosen to match onto the inner solution.
- <sup>38</sup> For most experimental systems, this regime  $r \gg R$  is not of physical interest, since the condensate density is vanishingly small there (e.g., for the TF  $\rho_s(r)$  profile). However, this regime may be accessible for condensate profiles with spatial variation on multiple length scales, such as  $\rho_s(\mathbf{r})$  with a Gaussian “bump” on top of a uniform profile varying on long length scales, as considered in Sec. V B 3 in the case of *many vortices* in an inhomogeneous condensate.
- <sup>39</sup> Vinay Ambegaokar, B.I. Halperin, David R. Nelson and Eric D. Siggia, Phys. Rev. B **21**, 1806 (1980).
- <sup>40</sup> See, e.g., Ping Ao and David J. Thouless, Phys. Rev. Lett., **70**, 2158 (1993).
- <sup>41</sup> For the case of a uniform lattice ( $\mathbf{u} = 0$ ), Tkachenko<sup>17</sup> has shown that Eq. (64a) along with Eq. (66) emerges formally from a small- $z$  expansion of his exact expression for the phase gradient of a uniform vortex array written in terms of the Weierstrass zeta function  $\zeta(z)$ .
- <sup>42</sup> Gordon Baym and Elaine Chandler, J. Low Temp. Phys. **50**, 57 (1983).
- <sup>43</sup> Uwe R. Fischer and Gordon Baym, Phys. Rev. Lett. **90**, 140402 (2003).
- <sup>44</sup> Within our continuum (density-functional) approximation the energy functional  $E[\mathbf{u}]$  only depends on the vortex density  $n_v(r)$  and is therefore independent of the transverse component of the phonon field  $\mathbf{u}_T$ .
- <sup>45</sup> Tin-Lun Ho, Phys. Rev. Lett. **87**, 060403 (2001).
- <sup>46</sup> C.B. Hanna, A.J. Sup, J.C. Diaz-Velez, J. Sinova and A.H. MacDonald, Bull. Am. Phys. Soc. P28.002 (2004).
- <sup>47</sup> Y. Shin, M. Saba, T.A. Pasquini, W. Ketterle, D.E.

- Pritchard and A.E. Leanhardt, Phys. Rev. Lett. **92**, 050405 (2004).
- <sup>48</sup> V.K. Tkachenko, Zh. Eksp. Teor. Fiz. **50**, 1573 (1966) [Sov. Phys. JETP **23**, 1049 (1966)]; Zh. Eksp. Teor. Fiz. **56**, 1763 (1969) [Sov. Phys. JETP **29**, 945 (1969)].
- <sup>49</sup> Gordon Baym, Phys. Rev. Lett., **91**, 110402 (2003).
- <sup>50</sup> E.B. Sonin, cond-mat/0405474.
- <sup>51</sup> Quantitative measurement of the rotation rate  $\Omega$  is in fact quite difficult, as it is typically experimentally determined by the cloud aspect ratio with error bars that grow with decreasing  $\Omega$ <sup>6,7</sup>.
- <sup>52</sup> Dietrich Stauffer and Alexander L. Fetter, Phys. Rev. **168**, 156 (1968).